Targeting PDAC Survival and Metastasis with Anacardium occidentale: Network Pharmacology and Structural Insights

Anindita S Raju
Vellore Institute of Technology University
Sadhana Balaji
Vellore Institute of Technology University
Gayathri Chandren
Vellore Institute of Technology University
Janaki Ramaiah Mekala
janakiramaiah.m@vit.ac.in

Vellore Institute of Technology University

Research Article

Keywords: Pancreatic ductal adenocarcinoma, Anacardium occidentale, Network pharmacology, Molecular docking, Monoterpenoids, PI3K-Akt signaling, MMP9, AKT1, Carvacrol, Phytochemicals

Posted Date: July 10th, 2026

DOI: https://doi.org/10.21203/rs.3.rs-10239598/v1

Additional Declarations: No competing interests reported.

Targeting PDAC Survival and Metastasis with Anacardium occidentale: Network Pharmacology and Structural Insights

Anindita S Raju[1], Sadhana Balaji[1], Gayathri Chandren[1], Janaki Ramaiah Mekala[1#]

[1] Department of Integrative Biology, School of Biosciences and Technology, Vellore Institute of Technology, School of Biosciences and Technology, Vellore Institute of Technology (VIT), Vellore - 632014, Tamil Nadu, India.

ABSTRACT

Pancreatic ductal adenocarcinoma (PDAC) remains one of the most lethal solid tumours, with a five-year survival below 12 percent and limited response to single-target therapeutics owing to its dense desmoplastic stroma and multi-driver oncogenic architecture. Natural-product polypharmacology offers an attractive alternative to conventional single-target agents. Here, we present an integrated computational framework combining network pharmacology, molecular docking, 100 ns molecular dynamics (MD) simulation, free energy landscape (FEL) analysis, and MM-PBSA (Molecular Mechanics Poisson–Boltzmann Surface Area) binding free energy calculations to evaluate the anti-PDAC potential of *Anacardium occidentale* (cashew) phytochemicals. From 399 phytochemicals curated from Dr. Duke's and IMPPAT 2.0 databases, ADME filtering and target-overlap analysis with PDAC-associated genes converged on six centrality-validated hub proteins; AKT1, SRC, EGFR, STAT3, IL6 and MMP9, enriched predominantly within PI3K-Akt, HIF-1 and focal-adhesion signalling. Molecular docking identified carvacrol and thymol as the strongest MMP9 ligand and pulegone as the top AKT1 binder. Subsequent MD simulation and MM-PBSA analysis confirmed carvacrol's superior thermodynamic stability at MMP9 (ΔG_{TOTAL} = −26.44 kcal/mol) relative to its structural isomer thymol (−14.68 kcal/mol), driven by a persistent Met422 hydrogen bond and favourable electrostatic contributions. Together, these convergent, multi-tiered results nominate carvacrol as a mechanistically validated, multi-target lead against PDAC invasion and survival signalling, and pulegone as a complementary AKT1-directed hit, providing a rational, thermodynamically grounded basis for future experimental validation.

Keywords: Pancreatic ductal adenocarcinoma, *Anacardium occidentale*, Network pharmacology, Molecular docking, Monoterpenoids, PI3K-Akt signaling, MMP9, AKT1, Carvacrol, Phytochemicals.

1. INTRODUCTION

Pancreatic ductal adenocarcinoma (PDAC) is a leading challenge in contemporary clinical cancer medicine, with its high prevalence and low responsiveness to therapeutic strategies resulting in a glaring mismatch. It is the 12th most common cause of cancer globally but remains the 6th most common cause of cancer-related deaths and the third most common cause of cancer-related deaths in the Western countries, indicating a significant disparity between prevalence and therapeutic efficacy . The clinical outlook for PDAC remains inefficient, with a five-year survival of 11% and minimal improvements over the last 40 years despite substantial research efforts. This is due to several inherent biological characteristics, such as its retroperitoneal location which impairs early detection, its rapid biology which allows early dissemination and the unique desmoplastic stroma that serves as a physical and chemical barrier to traditional chemotherapy drugs (Mehra et al., 2021).

The molecular biology of PDAC is extremely complex but driven by a "big four" of driver mutations; KRAS, TP53, CDKN2A, SMAD4, which coordinate tumor progression and resistance. This includes highly prevalent activating mutations in the KRAS oncogene (present in more than 90% of patients), the most primitive genetic lesion in early pancreatic lesions like the pancreatic intraepithelial neoplasia (PanIN) (Javadrashid et al., 2021). These mutations, typically in codons G12D or G12V, block the intrinsic GTPase activity of the Ras protein, resulting in constitutive activation of downstream RAF/MAPK/extracellular signal-regulated kinase (ERK) and PI3Ks/Akt/mTOR signaling pathways (Javadrashid et al., 2021). After KRAS activation, the loss of function of tumor suppressor genes, TP53 (~50-90% of patients), CDKN2A/p16 (~95% of patients), and SMAD4/DPC4 (~55% of patients) creates a selection of pressure for the development of invasive adenocarcinoma. These mutations combine to promote sustained growth, resistance to cell death, and metabolic adaptation, making the tumor refractory to the current standard of care, which is mainly based on the nucleoside analogue gemcitabine. Efforts to overcome the challenges of monotherapies have seen a rapid rise in the exploration of natural products as multi-target inhibitors. Herbal medicines are a treasure trove of secondary metabolites

that have evolved to bind to several targets, often called polypharmacology. Recent models have also employed integrated computational methods to validate the mechanism of action of these bioactive (Zhang et al., 2022). For example, an integrated in silico analysis identified APOE4, BACE1, TREM2, IL-1β, and TNF-α as key regulatory targets associated with amyloid beta–mediated immune dysregulation and neuroinflammation in Alzheimer's disease, while genkwanin and kaempferol demonstrated strong binding affinity toward these targets (Kalidass & Muthukaliannan, 2026). Similarly, a combined network pharmacology approach was used to assess the efficacy of Acalypha indica (Indian Nettle) against tuberculosis, revealing AKT1 and EGFR as hub foundation nodes in the protein-protein interaction network (Harakeh et al., 2024). Likewise, a study on luteolin from Annona muricata (Soursop) showed that the compound could act as a multi-target inhibitor for PDAC, via the MET/PI3K/AKT pathway (Mathpal et al., 2025).

These reports highlight the value of integrating network pharmacology, KEGG pathway analysis and molecular docking to disentangle the herbal bioactive-disease genes association network. Network pharmacology, as an integrated systems biology approach, is a successful transformation of drug discovery from the conventional "one drug, one target" approach to a "network target, multi-component" approach (Shi et al., 2023). This strategy is of particular importance for multifactorial diseases such as PDAC, where single-gene disorders are uncommon, and the disease is a consequence of the disruption of large gene networks. Through the development of a network model of interactions between active compounds and target proteins, the potential targets and mechanisms of action of natural products can be predicted with high accuracy. In this study, we examine the properties of Anacardium occidentale (Cashew), a plant known for its nutritional and biological activity, and its rich content of phenolic lipids and flavonoids with strong antioxidant, anti-inflammatory and cancer-preventing properties (Liu, Wang, et al., 2020).

Anacardium occidentale L. (Anacardiaceae), a tropical tree originally found in Brazil, is now widely cultivated around the world. Different parts of the cashew plant, such as the leaves, bark, fruits (cashew apple), and cashew nut shells, have been used in traditional medicine for a long time. Its leaves contain a variety of bioactive compounds, including quercetin glycosides, kaempferol, and tannins, which exhibit antimicrobial, anti-inflammatory, and cytotoxic effects. The cashew nut shell liquid (CNSL) is a rich source of a distinct type of phenolic lipids (anacardic acids, cardanols, and cardols) known for their potent histone acetyltransferase (HAT) enzyme

inhibition and cell cycle regulation These attributes make Anacardium bioactives potential candidates for multi-targeted therapies in PDAC, similar to other high-impact plant studies which display systemic regulatory effects (Shi et al., 2023).

2. MATERIALS AND METHODS

2.1 Retrieval of Phytochemicals

A comprehensive list of phytochemicals found in *Anacardium occidentale* was obtained from two ethnopharmacological databases. The Dr. Duke's Phytochemical and Ethnobotanical Database, an ethnobotanical database that combines information on phytochemicals and ethnomedicinal uses, was searched (https://phytochem.nal.usda.gov/, accessed on 19 January 2026) to retrieve the complete list of all plant natural chemical compounds reported for *Anacardium occidentale* (Wang et al., 2020). The Indian Medicinal Plants, Phytochemistry, and Therapeutics Database (IMPPAT 2.0) was also searched (https://cb.imsc.res.in/imppat/, accessed on 19 January 2026) to obtain further phytochemical details. The data sets from the two sources were combined, and duplicate entries were eliminated to obtain a list of unique phytochemical constituents reported in *Anacardium occidentale* (Chen et al., 2023).

2.2 Data Curation and Filtering

To ensure the removal of non-drug-like or structurally unfavorable molecules, the merged dataset of phytochemicals from *Anacardium occidentale* was curated through a curation workflow. Inorganic metals, non-metal elements, and proteinogenic amino acids (20 amino acids commonly found in proteins) were removed from the dataset because they do not possess the structural intricacy to interact with regular small-molecule drugs. This allowed us to include only structurally pertinent phytochemicals for further analysis. For each of the remaining compounds, searches in the PubChem database (https://pubchem.ncbi.nlm.nih.gov/, accessed on 20 January 2026) using their IUPAC names or synonyms were performed to obtain the PubChem Compound Identifiers (CIDs) for these compounds (Liu, Zhao, et al., 2020). Phytochemicals that failed to produce a valid CID, suggesting uncharacterized or poorly defined compounds, were removed from the dataset, leaving a final set of curated phytochemicals (Kim et al., 2023).

The canonical Simplified Molecular Input Line Entry System (SMILES) strings for all such compounds were then extracted from PubChem using their CIDs, as these SMILES strings are crucial for further computational investigations, such as Absorption, Distribution, Metabolism, and Excretion (ADME) profiling and target prediction (Daina et al., 2017).

2.3 ADME-Based Drug-likeness Screening

The canonical SMILES of phytochemicals from *Anacardium occidentale* were entered on the SwissADME web server (http://www.swissadme.ch/, accessed on 31 January 2026), a popular tool to estimate the pharmacokinetics and drug-likeness of small molecules. For all molecules, the molecular weight, lipophilicity (consensus Log P), hydrogen bond donor and acceptor numbers, topological polar surface area (TPSA), gastrointestinal (GI) absorption, blood-brain barrier (BBB) penetration, potential to be a P-glycoprotein (P-gp) substrate, and inhibition of cytochrome P450 (CYP) enzymes were examined (Daina et al., 2017). The compounds were then filtered according to Lipinski's Rule of Five, which defines the parameters of molecular weight $\leq$ 500 Da, LogP $\leq$ 5, hydrogen bond donors $\leq$ 5, and hydrogen bond acceptors $\leq$ 10. Compounds that triggered the Pan-Assay Interference Compounds (PAINS) or Brenk alert, suggesting chemically reactive or promiscuous scaffolds, respectively, were also removed. Using this "poly-parameter" screening method, the remaining phytochemicals were classified as drug-like compounds and chosen for further analysis.

2.4 Target Prediction for Drug-like Phytochemicals

To determine the possible molecular targets of the drug-like phytochemicals from *Anacardium occidentale*, the canonical SMILES of the compounds were uploaded to the SwissTargetPrediction server (http://www.swisstargetprediction.ch/, accessed on 5 February 2026), which employs a combination of chemical similarity and machine learning techniques to predict probable protein targets. The list of predicted targets was narrowed down to those of *Homo sapiens* only to ensure relevance to humans. The results were filtered using a threshold probability score to weed out spurious predictions, thus enhancing the quality of the data. Finally, the identified protein targets were filtered to remove duplicates, resulting in a list of unique protein targets for further analysis (Gfeller et al., 2014).

2.5 Identification of PDAC-Associated Disease Targets

We systematically extract disease-specific gene targets related to Pancreatic ductal adenocarcinoma (PDAC) from curated databases to provide comprehensive and accurate coverage of disease-related gene targets. The GeneCards database (http://www.genecards.org/, accessed on 17 February 2026) is an integrated database that aggregates gene-specific data from a variety of genomic, transcriptomic, proteomic and disease-specific databases, was searched with the terms "pancreatic cancer" and "pancreatic ductal adenocarcinoma" (Safran et al., 2021). GeneCards also include relevance scores, which are used to prioritize the most relevant genes associated with the disease of interest. The genes identified from these queries were collated into a single list. The list of genes was then curated to eliminate redundancies and harmonize the gene names, yielding a streamlined, unique list of PDAC-specific gene targets. This refined gene list was then employed for further analyses, such as identification of target overlap and pathway enrichment analyses.

2.6 Identification of Overlapping Targets

To discover pharmacologically significant intersecting targets, the protein targets of the phytochemicals of *Anacardium occidentale* and the compiled list of Pancreatic ductal adenocarcinoma (PDAC) target genes were compared via Venn diagrams. This was done using the Venny 2.1 tool (https://bioinfogp.cnb.csic.es/tools/venny) or a similar bioinformatics program. The intersection of the two sets corresponds to the common targets that may be involved in both the mechanism of action of Anacardium occidentale phytochemicals and PDAC disease. These common targets were extracted and identified as potential targets for drug development, which were further used for network and functional analyses.

2.7 Protein–Protein Interaction (PPI) Network Construction and Analysis

The common candidate targets of phytochemicals from *Anacardium occidentale* and Pancreatic ductal adenocarcinoma (PDAC) were entered into the STRING database (version 11.5; https://string-db.org/) with Homo sapiens selected as the organism to build a protein-protein interaction (PPI) network (Szklarczyk et al., 2023). We used a stringent interaction score cut-off (≥ 0.700) to include only significant interactions. The network data (nodes and edges) were exported in TSV format and imported into Cytoscape (version 3.7.2; https://cytoscape.org/) to conduct a topological analysis and identify hub genes (Shannon et al., 2003).

In Cytoscape, the cytoHubba plugin was used to determine the important nodes in the network based on three topological parameters: Maximal Clique Centrality (MCC), a measure of nodes that belong to the largest clique (complete sub-graph) in the network, Maximum Neighbourhood Component (MNC), a measure of the size of the largest connected component within a node's neighbourhood and Betweenness Centrality, a measure of the degree to which a node lies on the shortest paths between other nodes, implying that the node can be a "bottleneck" in the network. The common subset of the top ranked genes from the above three parameters was defined as the core set of hub genes, which are potential therapeutic targets mediating the pharmacological activity of *Anacardium occidentale* in PDAC (Chin et al., 2014).

2.8 KEGG Pathway Enrichment Analysis

To understand the biological functions of the common targets and to identify signaling pathways associated with the phytochemicals of *Anacardium occidentale* in Pancreatic ductal adenocarcinoma (PDAC), functional enrichment analyses were conducted. The STRING database was used to obtain (https://string-db.org/) Kyoto Encyclopedia of Genes and Genomes (KEGG) pathway enrichment analyses. KEGG pathway analysis was performed to map target molecules against known signaling and metabolic pathways to provide insights into their roles in disease-related biological pathways. The statistical significance was set at p-value < 0.05, and multiple hypothesis testing correction was performed using the Benjamini-Hochberg procedure (false discovery rate, FDR) to limit false positives. The enriched KEGG pathways were then visualized in the form of bar and dot plots, and enrichment maps to aid in interpretation and the identification of major biological processes and pathways (Kanehisa et al., 2023).

2.9 Molecular Docking

The top hub proteins identified from protein-protein interaction networks and pathway enrichment analysis of the phytochemicals from *Anacardium occidentale* and Pancreatic ductal adenocarcinoma (PDAC) were chosen for molecular docking simulations. Crystal structures of the selected target proteins were obtained from the RCSB Protein Data Bank (https://www.rcsb.org/). The target proteins and their PDB IDs are IL6:1ALU, SRC:1FMK, EGFR:2ITN, AKT1:4EJN, STAT3:6NJS. The AlphaFold Id of MMP9 used for docking and simulation study was AF-P14780-F1. The target proteins were processed using AutoDock Tools (version 1.5.7) by removing

water molecules, adding polar hydrogens and assigning Kollman united atom type charges to the protein. The binding pockets of the proteins were determined from the coordinates of the co-crystallised ligands (Wishart et al., 2018).

Ligand files of the phytochemicals were prepared from the canonical SMILES using Open Babel (version 3.1), with energy minimization, tautomerization and charge assignment using the MMFF94 force field. The protein-ligand complexes were docked using AutoDock Vina (version 1.2), with the active site of each protein as the centre of the grid box. Docking poses were ranked according to their binding affinity scores (kcal/mol).

2.10 Protein–Ligand Interaction Analysis

Docking-pose interaction analysis was conducted by two different tools to determine the interaction profiles of *Anacardium occidentale* phytochemicals with protein targets. The Protein-Ligand Interaction Profiler (PLIP) server (https://plip-tool.biotec.tu-dresden.de/) was utilised to systematically detect and classify non-covalent interactions between each docked phytochemical and its corresponding protein target. The interactions included hydrogen bonds (donor-acceptor distance and angle), hydrophobic, π-π stacking, π-cation, salt bridges, and halogen bonds. The interaction results were exported as XML/text reports and visualised as two-dimensional interaction maps (Salentin et al., 2015).

Meanwhile, BIOVIA Discovery Studio Visualizer (version 21.1; Dassault Systèmes) was used for the three-dimensional visualisation of docking poses and to generate fine-tuned two-dimensional ligand-receptor interaction maps. This software allowed us to identify critical amino acid residues participating in hydrogen bonding, hydrophobic interactions, π-interactions, and electrostatic interactions with each phytochemical ligand. The integration of PLIP and Discovery Studio served as a powerful and complementary approach to determine the interaction and stability of phytochemicals bound to active sites of the identified hub protein targets.

2.11 Molecular Dynamic Simulation

The complexes of MMP9-Carvacol and MMP9-Thymol were simulated using molecular dynamics (MD) in the GROMACS (2023.1) version to investigate the structural stability, conformational dynamics and intermolecular interactions of the docked complexes under physiologically relevant conditions (Abraham et al., 2015). Molecular docking gives us detail of the optimal binding

orientation of a ligand in the active site of a target protein that is in the energy minimised state, but it does not give a dynamic view of the evolution of the protein-ligand system in time. Hence, MD simulations complement docking studies by using Newton's classical equations of motion to determine the time-dependent atomistic behaviour of the solvated system, which also provides dynamic information that is more representative of physiological conditions.

The CHARMM-GUI online server was used to generate the force field parameters of each ligand in combination with the CHARMM36m all atom additive force field, which is more accurate for modelling folded proteins and intrinsically disordered regions (Huang et al., 2017). Ligand topology and the partial charge assignment was performed in the CHARMM-GUI Ligand Reader and Modeller module using the CGenFF parameterisation protocol (Vanommeslaeghe et al., 2010).

A rectangular periodic simulation box with at least 10 Å distance in all Cartesian directions was used for each protein-ligand complex. The systems were solvated with the standard three-site water model, TIP3P, that is compatible with the CHARMM36m force field. The charge neutrality of the system was realised by the addition of Na^+ or Cl^- counter ions by means of Monte Carlo based protocol for ion placement implemented in the GROMACS program.

Each solvated system was then energy minimised using the steepest descent algorithm to aid in resolving steric clashes and optimising the overall system structure until the maximum force dropped below 1000 kJ mol^{-1} nm^{-2} followed by a 500 ps NPT equilibration at 310.15K and 1atm pressure allowing relaxation of the box volume before production simulation. To simulate the production, 100 ns simulations were performed under NPT ensemble conditions with constant number of particles (N), pressure (P) and temperature (T). The velocity-rescaling thermostat algorithm of Bussi, Donadio and Parrinello was used to maintain the system at 310.15 K without imposing the ergodicity constraints found in the simple velocity rescaling algorithm.7 The Berendsen barostat was used to keep the pressure at 1 atmospheric, while using isotropic pressure coupling for all of the simulation. Periodic boundary conditions and a real space cutoff of 1.0 nm were used for the computation of long-range electrostatic interactions by the Particle-Mesh Ewald (PME) algorithm9. Van der Waals and Coulombic interactions were short ranged with a cut-off distance of 1.0 nm. The geometry of covalent bond configurations containing a hydrogen atom

was restricted by implementing the Parallel Linear Constraint Solver P-LINCS ()10 to speed up the calculations and to allow for integration of Newton's equations of motion with a time step of 2 fs (Hess, 2008). After production simulations completed, water molecules and ions as solvent were removed from the trajectory files, and the translational and rotational motions were separated from the global motions to study the internal structural dynamics in detail. Trajectories were analyzed with built-in GROMACS analysis tools, which included root mean square deviation (RMSD) of the backbone, per-residue root mean square fluctuation (RMSF) of the Cα positions, solvent accessible surface area (SASA), number of intermolecular hydrogen bonds (IM-HB) that are occupied and Principal Component Analysis (PCA) on covariance diagonalisation of the Cα positions fluctuations.

2.12 The Molecular Mechanics/Poisson-Boltzmann Surface Area

To complement the structural insights obtained from MD simulations, binding free energy calculations were performed using the Molecular Mechanics Poisson–Boltzmann Surface Area (MM-PBSA) approach, as implemented in the gmx_MMPBSA (version 1.4.3) software package. The MM-PBSA method is a widely adopted end-state free energy approach that offers an advantageous balance between computational efficiency and thermodynamic accuracy, particularly well-suited for ranking and comparing the binding free energies of small-molecule ligands within protein active sites (Valdés-Tresanco et al., 2021).

The single-trajectory protocol was employed for all MM-PBSA calculations, wherein the receptor (MMP9), ligand (Carvacrol or Thymol), and protein–ligand complex conformations were all extracted from the same equilibrated MD trajectory of the bound complex. This approach minimises cancellation errors in internal energies and is the standard methodology for protein–small-molecule binding free energy estimation. A total of 1000 snapshots were extracted at uniform intervals from the last 50 ns of each production trajectory, a time window in which both complexes had demonstrably converged as evidenced by the plateau in backbone RMSD profiles. Solvent water molecules and counter-ions were stripped from each snapshot prior to energy evaluation.

The total binding free energy (ΔG_{bind}) was computed according to the thermodynamic cycle:

$$\Delta G_{bind} = (\Delta E_{MM}) + (\Delta G_{sol}) - T\Delta S$$

where ΔE_{MM} represents the molecular mechanics energy contribution in vacuo, comprising the sum of changes in van der Waals interactions (ΔE_{vdW}) and electrostatic interactions (ΔE_{ele}). ΔG_{sol} denotes the total solvation free energy, decomposed into polar (ΔG_{polar}) and nonpolar ($\Delta G_{nonpolar}$) components MM bonded nonbonded bonded vdW elec represented as:

$$(E_{MM}) = (E_{bonded}) + (E_{non\text{-}bonded}) = (E_{bonded}) + (E_{vdW} + E_{elec})$$

The entropic term ($-T\Delta S$) was not explicitly computed in the present study, consistent with the standard single-trajectory MM-PBSA protocol in which the conformational entropy contribution is assumed to cancel across analogous systems, a widely employed approximation when comparing ligands of similar size and flexibility.

The polar solvation free energy (ΔG_{polar}) was calculated by solving the linearised Poisson–Boltzmann (PB) equation using an internal dielectric constant of 2.0 for the protein–ligand complex and an external (solvent) dielectric constant of 80.0, values consistent with the standard parameterisation for condensed-phase biomolecular simulations. Ionic strength was set to 0.15 M to reflect physiological salt concentration.

The nonpolar solvation contribution ($\Delta G_{nonpolar}$) was estimated using the Solvent-Accessible Surface Area (SASA) model, in which the nonpolar free energy is expressed as a linear function of the solvent-accessible surface area:

$$\Delta G_{nonpolar} = \gamma \cdot SASA + \beta,$$

where γ is the surface tension coefficient (0.0227 kJ mol^{-1} Å^{-2}) and β is an offset constant (3.849 kJ mol^{-1}). The SASA was computed with a solvent probe radius of 1.4 Å using the fast Linear Combinations of Pairwise Overlaps (LCPO) algorithm.

To identify the specific residues of MMP9 that contribute most significantly to ligand binding, per-residue energy decomposition analysis was performed for each complex. Contributions from each residue were decomposed into van der Waals, electrostatic, polar solvation, and nonpolar solvation components, enabling a residue-level mapping of the binding hotspots and rationalisation of the differential binding affinities observed between Carvacrol and Thymol.

3. RESULTS

3.1 Phytochemical Collection and Data Curation

A total of 156 phytochemicals were retrieved from Dr. Duke's Phytochemical and Ethnobotanical Database, and 337 phytochemicals were obtained from the IMPPAT 2.0 database for Anacardium species. Upon merging both datasets and removing redundancies, 399 unique phytochemical entries were compiled. Subsequent exclusion of inorganic metals, elemental non-metals, and proteinogenic amino acids reduced the dataset to 338 phytochemicals. Cross-referencing against the PubChem database yielded valid SMILES for 311 compounds possessing confirmed PubChem CIDs, which were carried forward for ADME analysis.

3.2 ADME Screening and Drug-likeness Assessment

SwissADME evaluation of the 311 phytochemicals against Lipinski's Rule of Five and additional pharmacokinetic filters identified 146 drug-like compounds satisfying all criteria including high predicted gastrointestinal absorption, absence of PAINS and Brenk structural alerts, and acceptable bioavailability scores. The excluded 165 compounds were predominantly characterized by high molecular weights, excessive polar surface areas, multiple PAINS flags, or poor predicted oral bioavailability, rendering them unsuitable for further target-based analysis (Table 1).

Table 1: Summary of phytochemical collection and filtering pipeline

S.No	Stage	Database / Action	Count
1.	Initial collection	Dr. Duke's Phytochemical Database	156
2.	Initial collection	IMPPAT Database	337

S.No	Stage	Database / Action	Count
3.	After merging	Combined unique phytochemicals	399
4.	After filtering	Removal of metals, non-metals, common amino acids	338
5.	PubChem retrieval	Phytochemicals with valid PubChem CID	311
6.	After ADME screening	Drug-like phytochemicals (SwissADME)	146

3.3 Selection of Phytochemicals for Molecular Docking

Based on ADME profiles and reported bioactivities, six monoterpenoid phytochemicals were selected for molecular docking: **carvacrol, thymol, cuminal (cuminaldehyde), carvone, pulegone, and piperitone**. These compounds belong to the monoterpenoid phenol and ketone structural classes and share a common C_{10} isoprenoid scaffold. Carvacrol and thymol are structural isomers differing in the position of the hydroxyl group; both are well-established bioactive phenolic monoterpenes with documented anti-inflammatory and anti-proliferative activities (Table 2). Cuminal (cuminaldehyde) is an aromatic monoterpene aldehyde with reported anticancer and antidiabetic properties. Carvone, pulegone, and piperitone are enone-class monoterpenoid ketones with demonstrated cytotoxic and antifungal activities. All six compounds satisfy drug–likeness criteria and are characterised by low molecular weights (148–152 Da), favourable lipophilicity, and high predicted oral bioavailability.

Table 2: Selected phytochemicals for molecular docking and their physicochemical properties

S.No	Compound	MW	LogP	HBD	HBA	TPSA	GI absorption	BBB permeability	P-gp substrate	CYP inhibition
1.	Pulegone	152.23	2.32	0	1	17.07	High	Yes	No	No
2.	Piperitone	152.23	2.38	0	1	17.07	High	Yes	No	No
3.	Cuminaldehyde	148.2	2.03	0	1	17.07	High	Yes	No	No
4.	Carvone	152.23	2.37	0	1	17.07	High	Yes	No	No
5.	Carvacrol	150.22	2.24	1	1	20.23	High	Yes	No	Yes
6.	Thymol	150.22	2.23	1	1	20.23	High	Yes	No	Yes

3.4 Target Prediction and Overlapping Target Identification

Swiss Target Prediction analysis of the 146 drug-like phytochemicals yielded 557 unique human protein targets. Independent retrieval of PDAC-associated disease targets from GeneCards produced an initial dataset of 7,253 gene entries. Application of a GeneCards Relevance Score threshold of ≥ 20 reduced this to 807 high-confidence PDAC-associated targets, thereby eliminating peripheral and poorly evidenced gene associations. Venn diagram comparison of the 557 phytochemical targets with the 807 PDAC disease targets identified 91 overlapping targets, representing the pharmacologically relevant intersection of Anacardium phytochemical activity and PDAC pathogenesis (**Figure 1**). These 91 proteins were retained as priority therapeutic candidates for network analysis.

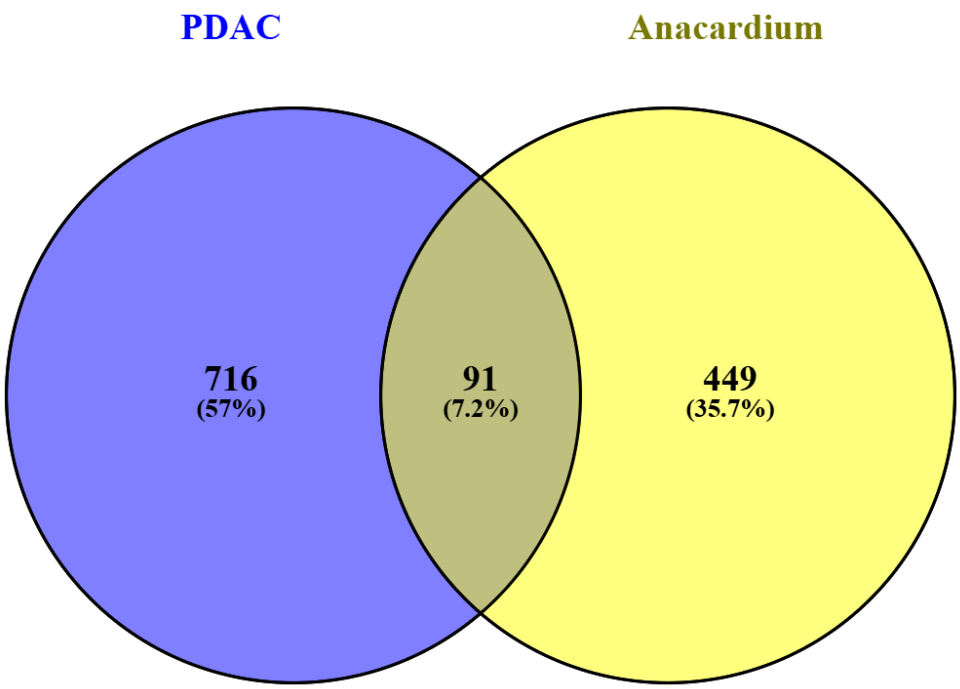

Figure 1. Venn Diagrm showing overlapping between phytochemical derived targets of Anacardium occidentale and PDAC associated genes. A total of 91 targets were identified, which may serve as putative targets of A. occidentale to exert their anti-PDAC effects.

3.5 PPI Network Analysis and Hub Gene Identification

STRING-based PPI network construction of the 91 overlapping targets generated a high-confidence interaction network (score ≥ 0.700), which was imported into Cytoscape for topological analysis using the cytoHubba plugin (**Figure 2**). Evaluation of all nodes using Maximal Clique Centrality (MCC), Maximum Neighborhood Component (MNC), and Betweenness centrality metrics consistently identified six proteins as the most topologically significant hub genes across all three scoring parameters.

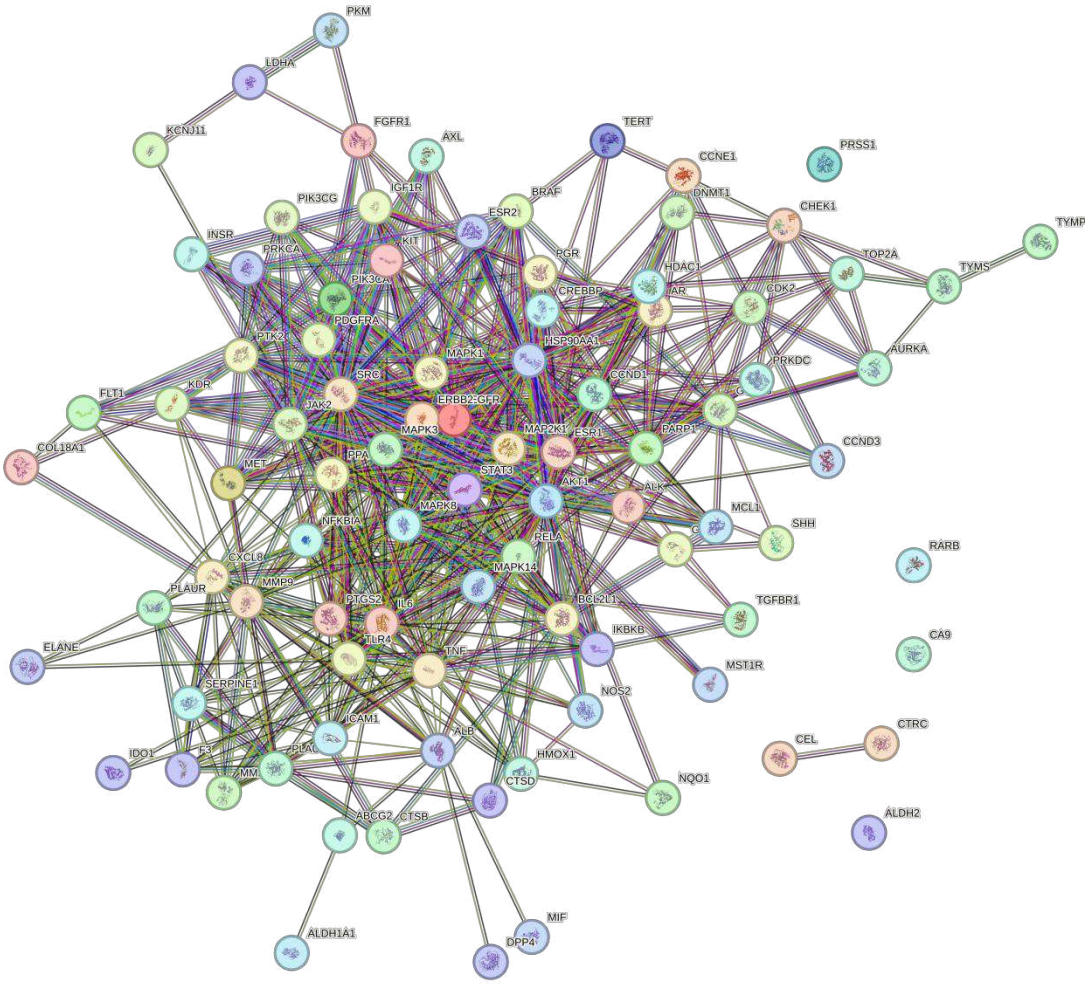

Figure 2. The Protein-Protein Interaction (PPI) network of the 91 overlapping targets was constructed using the STRING database. The nodes represent the proteins whereas the edges indicate interactions between the proteins

The six hub genes identified were (Figure 3), RAC-alpha serine/threonine-protein kinase (**AKT1)**, a central mediator of the PI3K-Akt survival pathway; proto-oncogene tyrosine-protein kinase Src (**SRC)**, a key regulator of cell adhesion and invasion signalling; Epidermal Growth Factor Receptor (**EGFR**), a receptor tyrosine kinase critically implicated in PDAC progression and therapeutic resistance; Signal Transducer and Activator of Transcription 3 (**STAT3**), a transcription factor mediating inflammatory and immune evasion signals in the PDAC tumour microenvironment; Interleukin-6 (**IL6**), a pro-inflammatory cytokine that activates STAT3 and promotes tumour cell survival; and Matrix Metallopeptidase-9 (**MMP9**), a key effector of extracellular matrix remodelling, tumour invasion, and metastasis. These six proteins were selected as receptor targets for molecular docking studies (**Table 3**).

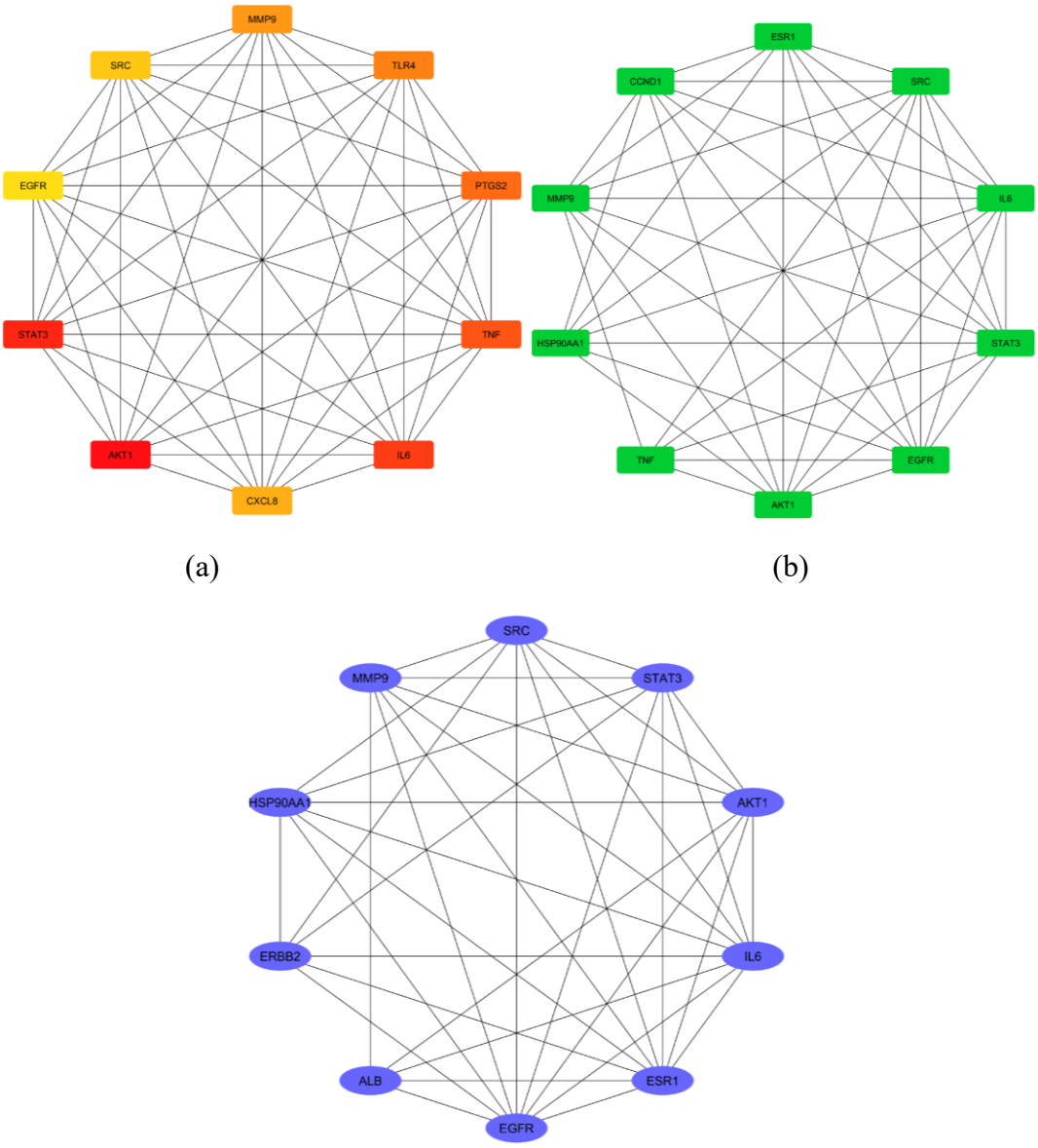

Figure 3. The network analysis of potential protein targets based on (a) MCC, (b), MNC and (c) Betweenness depicted in Red, Green and Blue respectively. In the network diagram, circular nodes represent individual proteins, while the connecting edges indicate documented protein-protein interactions sourced from the STRING database.

Table 3. Hub genes identified from PPI network analysis with MCC, MNC, and Betweenness centrality

Hub Gene	Full Name	MCC Rank	MNC Rank	Betweenness Rank	Biological Role in PDAC
AKT1	RAC-alpha serine/threonine-protein kinase	Top	Top	Top	Cell survival, proliferation, PI3K-Akt axis
SRC	Proto-oncogene tyrosine-protein kinase Src	Top	Top	Top	Signal transduction, invasion
EGFR	Epidermal growth factor receptor	Top	Top	Top	Cell growth, EGFR resistance pathway
STAT3	Signal transducer and activator of transcription 3	Top	Top	Top	Inflammation, immune evasion, survival
IL6	Interleukin-6	Top	Top	Top	Pro-inflammatory cytokine, STAT3 activator
MMP9	Matrix metallopeptidase-9	Top	Top	Top	ECM remodelling, invasion, metastasis

3.6 Drug Target Pathway Identification by Cytoscape

The mechanism of action of the bioactive compounds on PDAC is elucidated through Drug-Target-Protein (D-T-P) interactions (**Figure 4)**. It involves between 20 and 25 bioactive compounds such as Carvacrol, Thymol, Estragole, Nerol, trans-2-Hexenal, Anethole, Camphene, (−)-Pulegone, Methyl Salicylate, Cinnamaldehyde, Nonanal, 4-Methoxybenzaldehyde, Carvone, and beta-Cyclocitral. In addition, there were connections between 50 and 70 proteins that serve as targets for the disease as well as between 15 and 18 signaling pathways related to PDAC. Target layer contains several protein nodes with larger size implying that they are crucial for the pathogenesis of PDAC due to their high connectivity in the network. These important proteins mediate processes underlying PDAC such as cell proliferation, resistance to apoptosis, metastasis, and invasion. Analysis of pathways highlighted the connection to various major signaling pathways in PDAC including PI3K-Akt signaling pathway, KRAS-mutation induced EGFR/ErbB signaling, Wnt/β-catenin signaling, Proteoglycans in cancer, AGE-RAGE signaling pathway in diabetic complications, HPV-associated, and Fluid shear stress in fibrous tissue. Such interlinked pathways are important since bioactive compounds interact with the key elements that are causative to PDAC.

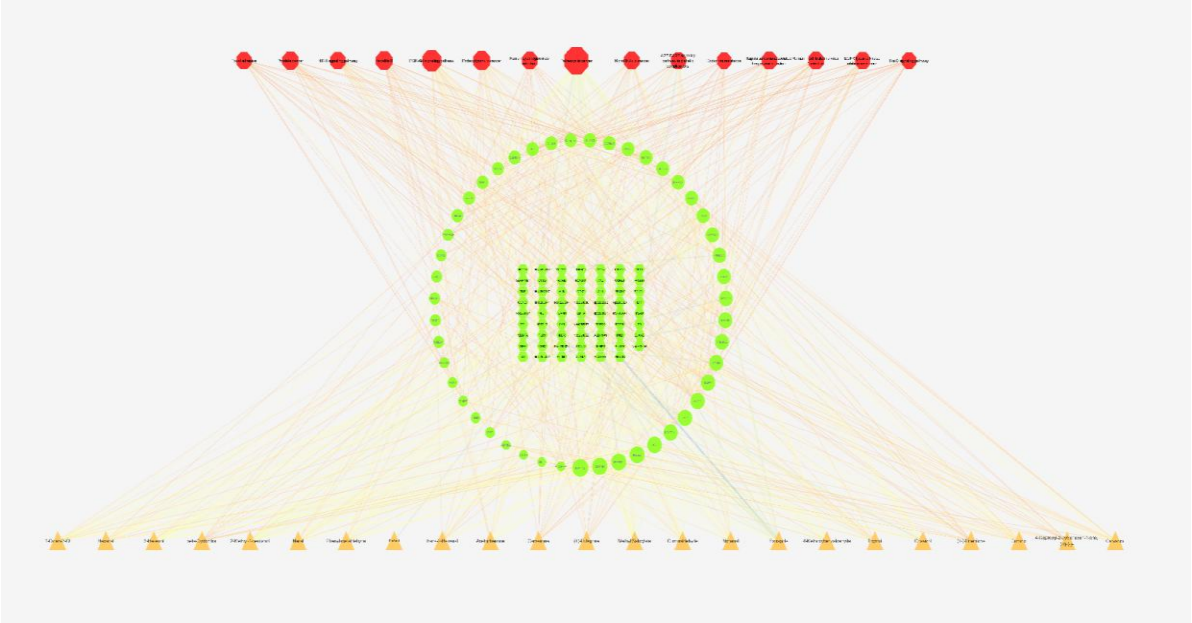

Figure 4. Drug target pathway interaction between bioactive compounds. The orange triangles at the bottom represent interaction among bioactive compounds, the green circle in the middle depicts protein targets, and the red circles at the top denote disease-associated pathways.

3.7 KEGG Pathway Enrichment Analysis

KEGG pathway enrichment analysis of the 91 overlapping targets identified 15 statistically significant pathways (adjusted $p < 0.05$). The most significantly enriched pathway was "Pathways in cancer" (hsa05200), a broad oncology meta-pathway encompassing multiple hallmark cancer processes. The PI3K-Akt signalling pathway (hsa04151) was prominently enriched, consistent with the identification of AKT1 as a central hub gene and reflecting the fundamental role of this axis in PDAC cell survival, proliferation, and resistance to apoptosis. The EGFR tyrosine kinase inhibitor resistance pathway (hsa01521) and Endocrine resistance pathway (hsa01522) further indicate that Anacardium phytochemicals may modulate clinically relevant drug resistance mechanisms in PDAC (**Table 6**).

In our studies we found that the HIF-1 signalling pathway (hsa04066) and Focal adhesion pathway (hsa04510) were significantly enriched, linking phytochemical target activity to tumour hypoxia adaptation and cancer cell invasion, respectively. The key processes that are closely associated with PDAC aggressiveness. The Forkhead box O (FoxO) signalling pathway (hsa04068), a key regulator of apoptosis and cell cycle arrest, suggests potential pro-apoptotic mechanisms for these

phytochemicals. Enrichment of Proteoglycans in cancer (hsa05205) implicates existence of extracellular matrix remodelling and modulating tumour microenvironment. The AGE-RAGE signalling pathway in diabetic complications (hsa04933) is of clinical relevance, given the well-documented mechanistic and epidemiological link between type 2 diabetes mellitus and elevated PDAC risk. MicroRNAs in cancer (hsa05206) suggest epigenetic and post-transcriptional regulation of oncogenes as an additional mechanism. The enrichment of several viral oncogenesis-related pathways including Hepatitis B (hsa05161), Kaposi sarcoma-associated herpesvirus infection (hsa05167), Human T-cell leukemia virus 1 infection (hsa05166), and Human cytomegalovirus infection (hsa05163) reflects the broad immunomodulatory capacity of Anacardium phytochemicals through shared oncoviral signalling intermediaries (Figure 5).

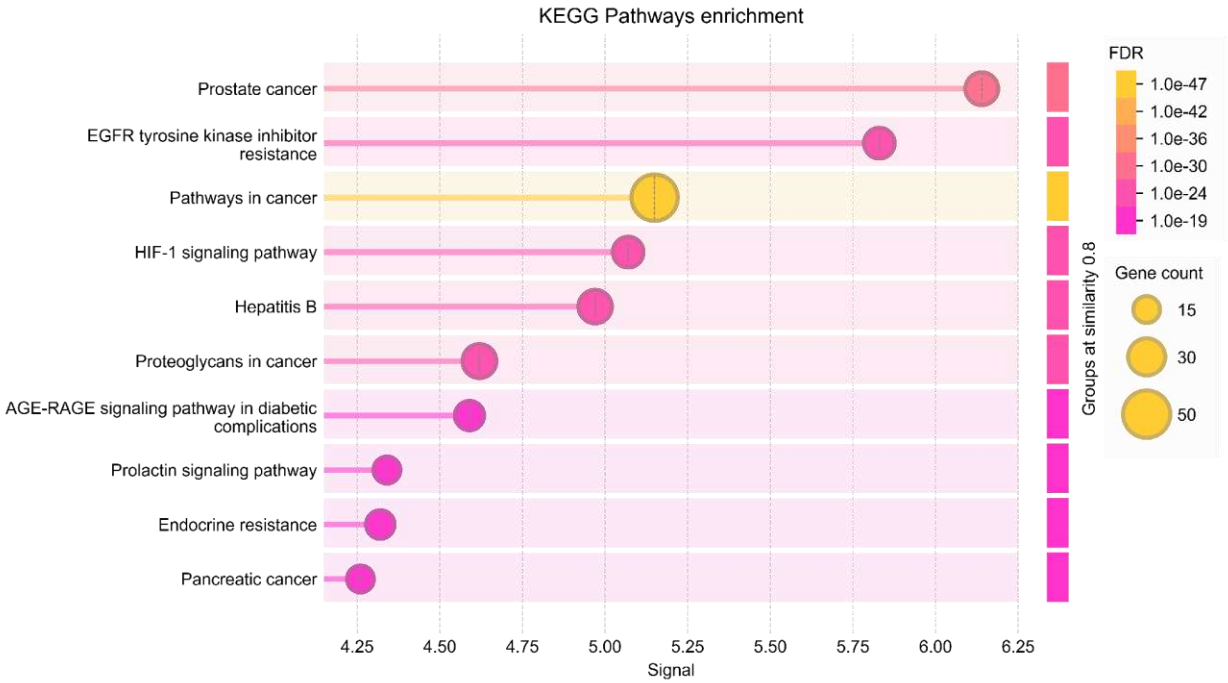

Figure 5. Bubble map visualization of enriched signaling pathways

3.8 Molecular Docking and Binding Thermodynamics of *A. occidentale* Phytochemicals

To better understand the therapeutic potential of phytochemicals from Anacardium occidentale against pancreatic ductal adenocarcinoma (PDAC), the molecular docking simulations were performed against six hub proteins namely, IL6, SRC, EGFR, AKT1, STAT3 and MMP9. The binding affinities, with the docking score (kcal/mol) calculated (**Table 4)**. The evaluated

phytochemical library showed a wide range of binding thermodynamics for the targeted proteins ranging from free energies of binding ΔG values −4.473 to −7.767 kcal/mol.

The docking matrix revealed that the most energetically favorable target for the phytochemicals tested was Matrix Metalloproteinase-9 (MMP9). Specifically, the complex of MMP9 with carvacrol resulted in the most negative binding energy of the study, at −7.767 kcal/mol, suggesting that it is a highly stable protein–ligand complex. Thymol (ΔG = −7.489 kcal/mol) and carvone (ΔG = −7.345 kcal/mol) showed this strong affinity for the MMP9 active site as well, indicating that these particular monoterpenoids have structural characteristics that are very complementary to the binding pocket of the enzyme.

Carcavrol is a significant multi-target compound from the library tested which is particularly associated with MMP9. It showed high binding affinity to SRC kinase (ΔG = −6.138 kcal/mol) and a significant binding affinity to AKT1 (ΔG = −6.659 kcal/mol). Similarly, pulegone showed a very good polypharmacological profile with the best docking score against AKT1 (ΔG = −6.960 kcal/mol) of all the compounds tested, and was the most strongly bound to STAT3 (ΔG = −5.202 kcal/mol), and tied with carvone for being the strongest interacting compound with EGFR (ΔG = −5.670 kcal/mol).

By contrast, the molecular interactions with Interleukin-6 (IL6) were the most unfavorable throughout the phytochemical panel. The docking score of IL6 fell within a small range of high energy values between −4.473 and −4.798 kcal/mol for the carvone and the carvacrol respectively. These relatively low binding energies suggest that these particular components of A. occidentale do not increase the likelihood of being strong and direct modulators of IL6, further demonstrating the target specificity these ligands have towards MMP9 and AKT1 (**Figure 6, Figure 7**).

Table 4. Binding Energy values of potent phytochemicals against the Hub-proteins

S.No	**Protein** with PDB ID	Carvacrol	Carvone	Cuminaldehyde	Piperitone	Pulegone	Thymol
1.	**IL6 (1ALU)**	-4.798	-4.473	-4.613	-4.605	-4.724	-4.531
2.	**SRC (1FMK)**	-6.138	-5.743	-5.691	-5.189	-5.455	-6.045
3.	**EGFR (2ITN)**	-5.48	-5.67	-5.243	-5.333	-5.67	-5.604
4.	**AKT1 (4EJN)**	-6.659	-6.536	-6.588	-6.836	-6.96	-6.614

5.	**STAT3 (6NJS)**	-5.109	-4.82	-5.025	-4.809	-5.202	-4.692
6.	**MMP9 (AF-P14780-F1)**	-7.767	-7.345	-7.233	-6.958	-5.83	-7.489

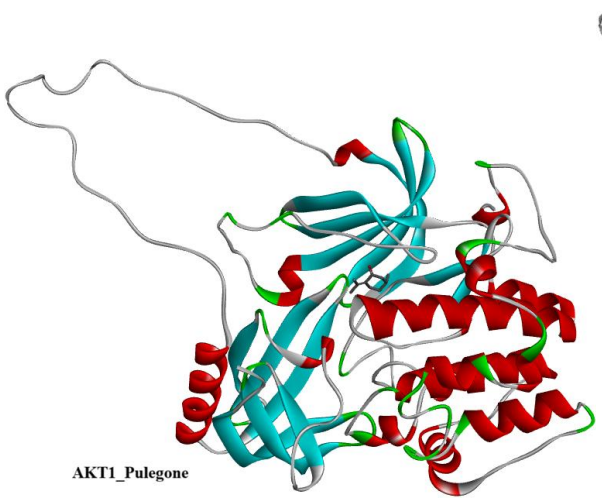
AKT1_Pulegone

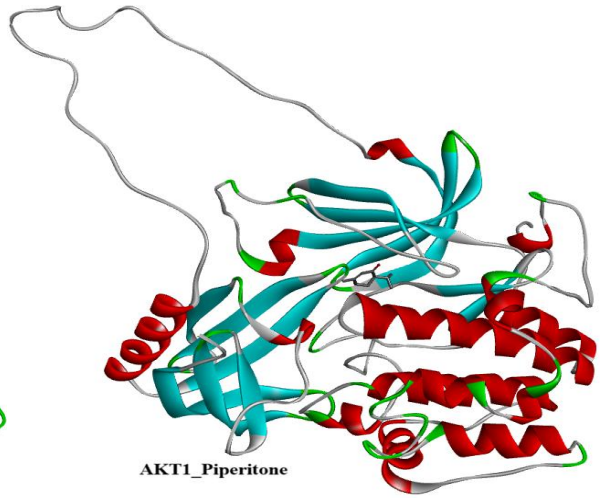
AKT1_Piperitone

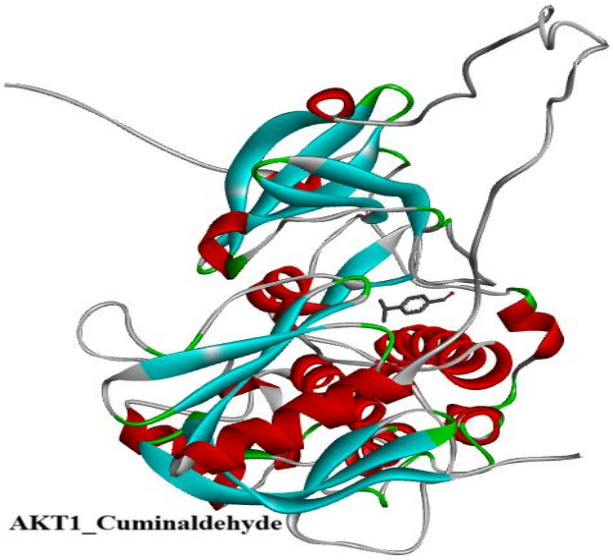
AKT1_Cuminaldehyde

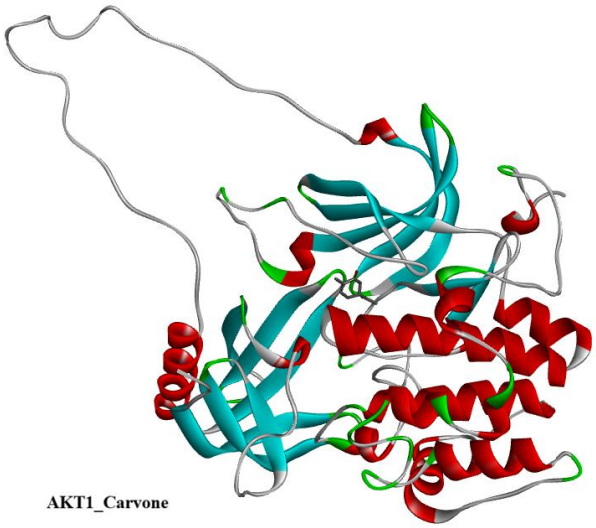
AKT1_Carvone

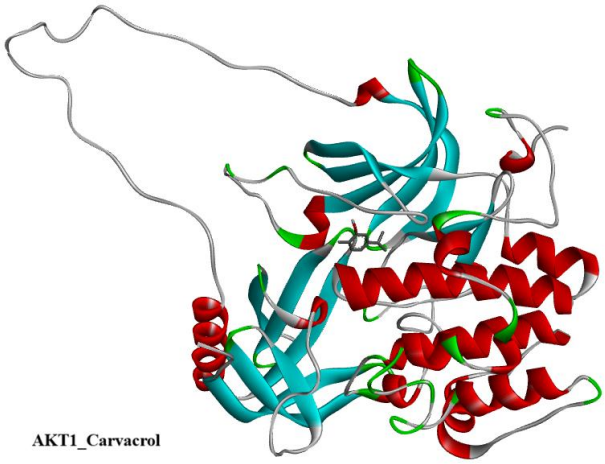
AKT1_Carvacrol

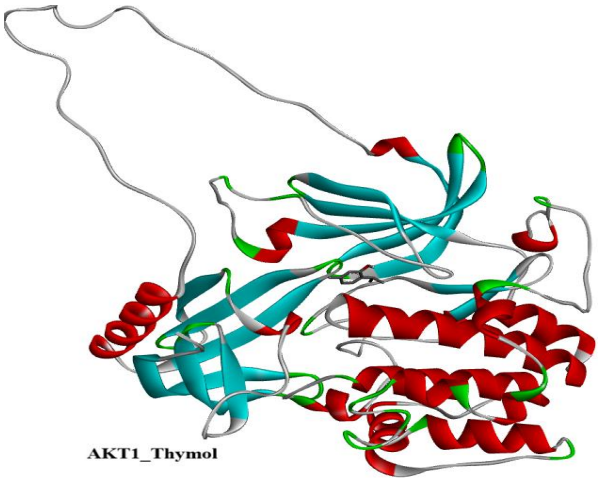
AKT1_Thymol

Figure 6. Docking complexes of AKT1 with the 6 active phytochemicals which include Pulegone, Piperitone, Cuminaldehyde, Carvone, Carvacrol, and Thymol

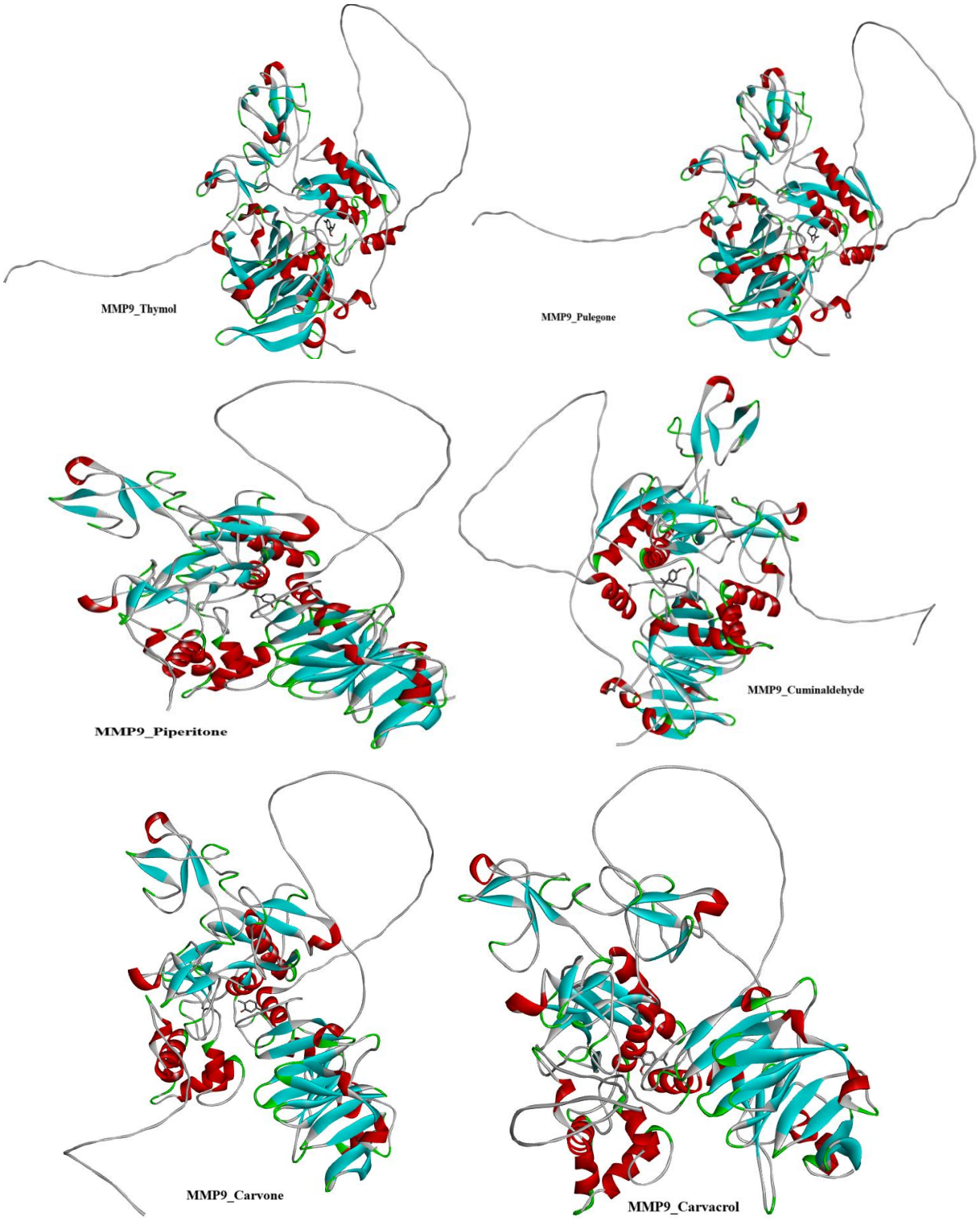

Figure 7. Docking complexes of MMP9 with the 6 active phytochemicals which include Pulegone, Piperitone, Cuminaldehyde, Carvone, Carvacrol, and Thymol

3.9 Protein Ligand interaction Analysis

To understand the specific non-covalent intermolecular forces that are responsible for the favorable binding thermodynamics observed during molecular docking simulation, two-dimensional (2D) interaction diagrams were generated and analyzed using BIOVIA Discovery Studio Visualizer for the top-scoring complexes. This structural analysis highlighted the key hydrogen bonds, hydrophobic contacts, and π-stacking interactions that stabilize the phytochemicals within the respective enzyme binding pockets. The most thermodynamically stable complex is carvacrol bound in the active site of MMP9, which is mainly stabilized by a tight hydrogen bond between this ligand and the Met422 residue (Table 5). This primary electrostatic contact is greatly augmented by a strong hydrophobic interaction network with residues Leu397, His401, Leu418, Tyr423 and Arg424 (Figure 9). The structurally related monoterpenoid, thymol, also bound in a similar fashion to Tyr420 and has a similar hydrophobic interaction profile with Leu397, Val398, Leu418, Tyr423, Arg424 and Thr426. Carvone, in contrast, does not form hydrogen bonding contacts with the protein, and the observed binding appears to be entirely hydrophobic, with the contacts involving Leu397, Val398, Leu418, Tyr423 and Thr426. The top ligands of the AKT1 target were found to bind to it in different ways through interaction profiling. The highest affinity ligand, pulegone, is stabilized by a large number of hydrophobic interactions with the residues Trp80, Leu210, Lys268 and Val270. In contrast, carvacrol's interactions with AKT1 involve a more complex array of intermolecular interactions. It makes a stabilizing hydrogen bond with Ser205 and has hydrophobic interactions with Trp80, Leu210, Leu264 and Lys268 (Figure 8). In addition, triterpenoids are also known for their ability to interact with the Trp80 residue to promote stabilization of π-stacking interactions, thereby enhancing their binding affinity. Moreover, triterpenoids are also known to interact with the Trp80 residue to promote the stabilization of π-stacking interactions, which enhances their binding affinity. Finally, the binding mode of carvacrol in the SRC kinase domain has been shown to be highly hydrophobic. The ligand makes good aliphatic and non-polar interactions with the residues of Leu192, Val200, Leu312 and Ala322, which fix it in the pocket.

Table 5. Key interactions between potent phytochemical and key regulatory proteins

Phytochemical	Protein	Hydrogen bond interactions	Other interacting atoms
AKT1	Carvacrol	SER205	TRP80, LEU210, LEU264, LYS268, VAL270, ASN204, GLN203, THR211, ASP292
	Carvone	SER205	VAL270, LYS268, TRP80, LEU264, TYR272, ASP292, LEU210, ASN204
	Cuminaldehyde	-	VAL270, LYS268, LEU264, TRP80, ASP292, ASN204, GLN203, TYR272
	Piperitone	SER205	LEU210, TRP80, LYS268, VAL270, LEU264, ASP292, THR211, ASN204
	Pulegone	SER205	LEU264, VAL270, LEU210, LYS268, TRP80
	Thymol	SER205	LEU264, TRP80, LYS268, VAL270, LEU210, ASN204
MMP9	Carvacrol	MET422	LEU418, VAL398, LEU188, TYR423, HIS401, LEU397, THR426, ARG424, MET422, PRO421, CYS99
	Carvone	-	THR426, ARG424, LEU418, TYR423, LEU397, VAL398, HIS401, LEU188, ALA417, MET422, TYR420, CYS99, PRO421
	Cuminaldehyde	-	CYS99, TYR423, HIS401, VAL398, LEU418, GLU402, PRO421, TYR420, MET422, ALA417, ARG424, THR426, ARG98, LEU188, LEU397
	Piperitone	TYR420	LEU418, TYR423, VAL398, HIS401, LEU397, ARG424, PRO430, THR426, ALA417, TYR420, MET422
	Pulegone	TYR420	HIS401, LEU418, LEU397, THR426, PRO430, GLU416, ALA417, PRO415, ARG424, VAL398, TYR423, MET422, TYR420

	Thymol	LEU418, ALA417, TYR420	THR426, LEU397, ARG424, LEU188, VAL398, HID40, MET422, TYR423, MET419

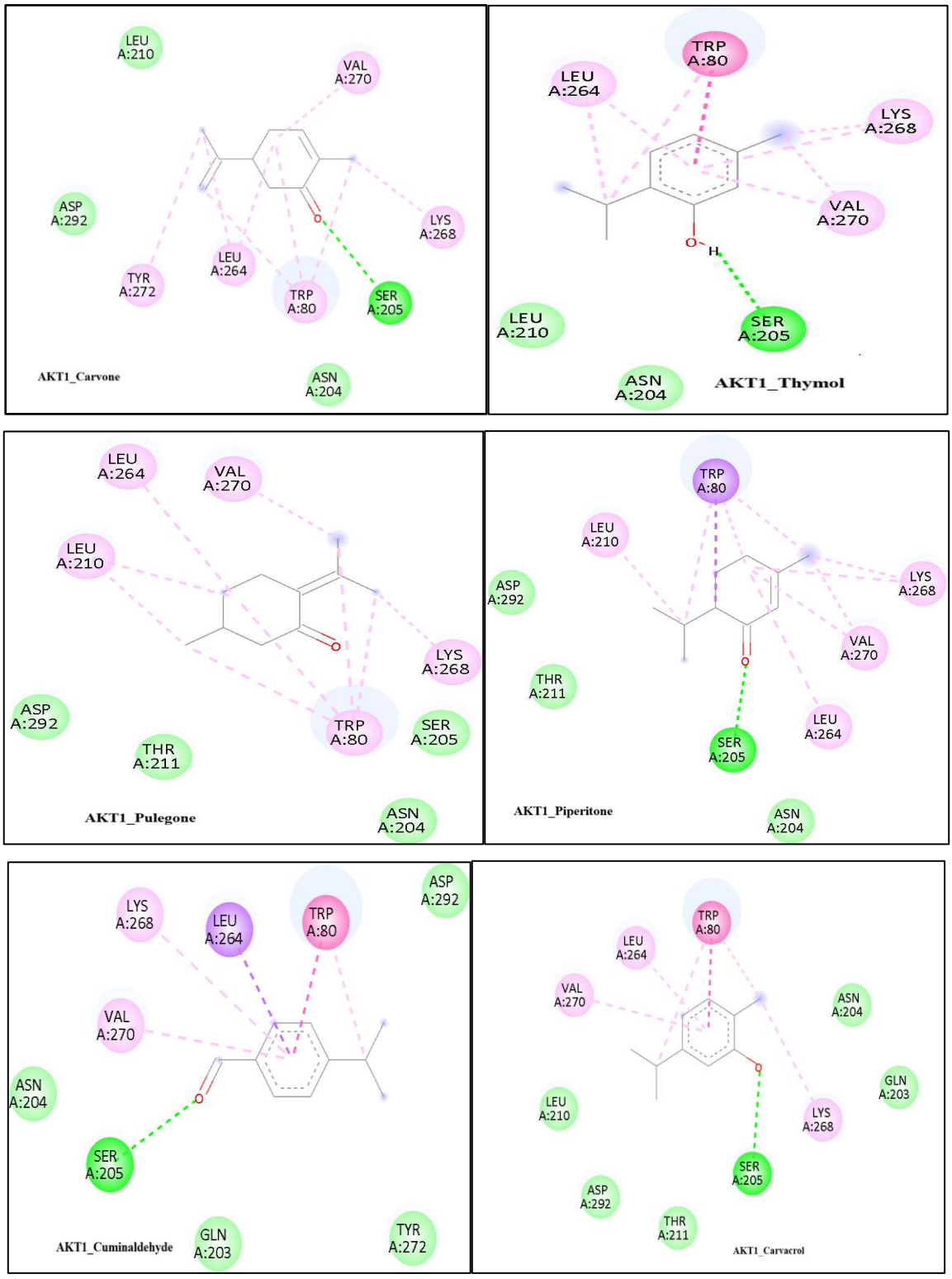

Figure 8. 2D representation of amino acid residue interacting from protein such as Thymol, Pulgene, Piperitone, Cumilaldehyde, Carvone, and Carvacol interacting with AKT1

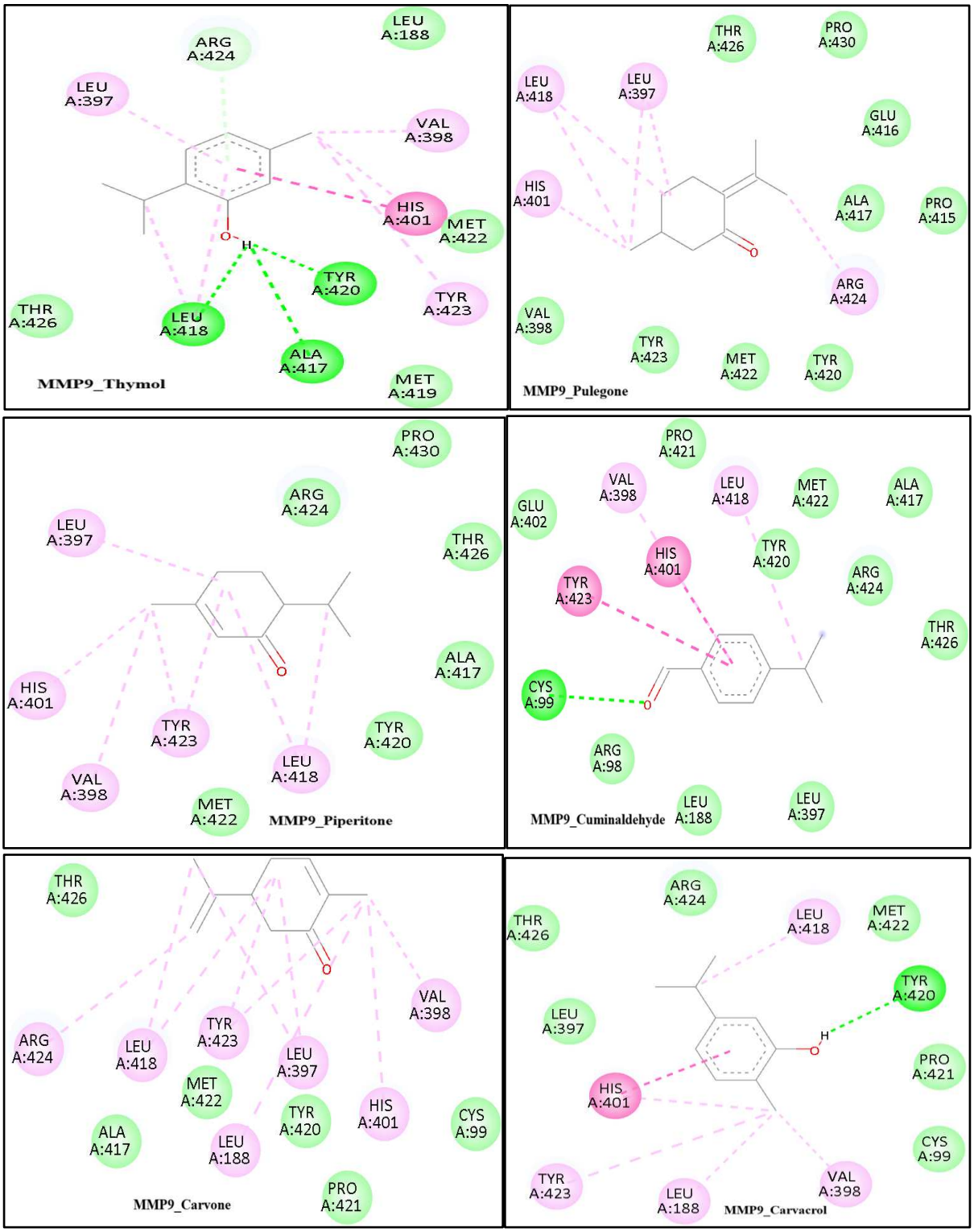

Figure 9. 2D representation of amino acid residue interacting from protein such as Thymol, Pulgene, Piperitone, Cumilaldehyde, Carvone, and Carvacol interacting with MMP9

3.10 Molecular Dynamic Simulation

Based on the molecular docking studies, the phytochemicals such as Carvacol and Thymol exhibited strong binding affinity against MMP9 which is a key protein for epithelial to mesenchymal transition. Using the Gromacs-2023.1 version, the conformational stability and intra-molecular interactions were studied by molecular dynamic simulation. In this study, a 100 ns molecular dynamic simulation of the docked complexes was performed to understand these conformational dynamics and intra-molecular interactions induced by the binding of the ligand.

The analysis of the Root Mean Square Deviation (RMSD) trajectories demonstrated that each complex has passed an equilibration phase at the beginning of the simulation, followed by stabilization. Nonetheless, significant differences have been observed between the two complexes. The MMP9-Carvacrol complex was characterized by lower RMSD values, with deviations not exceeding 2 nm in most of the simulations, while MMP9-Thymol underwent significant deformations from the initial structure, increasing up to 2.7 nm at the end of the simulation.

The degree of conformational mobility of individual residues was assessed through Root Mean Square Fluctuation (RMSF) analysis. According to the results obtained, the MMP9-Carvacrol complex has lower RMSF values, indicating restricted local motions of the residues and high conformational stability of the structure. On the contrary, MMP9-Thymol was characterized by higher RMSF values, which demonstrate greater structural dynamics and increased local motion of residues, especially in the region of residues about 450-720. Thus, it can be concluded that the presence of Carvacrol in the binding pocket contributes to increased structural stability, which is associated with the reduction of flexibility.

For the evaluation of the compactness of the structures during MD simulations, the radius of gyration was used. It was shown that the radius of gyration in the MMP9-Carvacrol complex gradually decreased from about 3.15 nm to 2.85 nm, which is a consequence of the increase in compactness and stability of the protein molecule. As for MMP9-Thymol, its Radius of gyration (Rg) values did not change much and were higher with respect to the former complex. Consistently, according to the Solvent Accessible Surface Area (SASA), there was a tendency of progressive reduction of solvate accessible surfaces in both complexes over time; still, MMP9-Carvacrol had a slightly smaller SASA in the latter parts of the simulations.

By considering SASA and Rg values, the following conclusions can be drawn: Carvacrol promotes the formation of a more condensed and structurally stable MMP9 complex than Thymol.

In addition to analyzing SASA and Rg values, it was decided to examine hydrogen bonding in each system to get further evidence on whether complexes with each ligand are stable or not (**Figure 10**). Each complex was characterized by one to three hydrogen bonds formed between MMP9 and the respective ligand. Although the number of possible hydrogen bonds is limited in such small molecules, hydrogen bonding occurs constantly throughout the whole simulation time, which means that the ligands persistently occupy the binding cavity.

To evaluate global motion in both systems, PCA was applied. Trajectories were projected to the first two PCs (PC1 and PC2) and compared visually to reveal any significant differences between the complexes with the two ligands. It is important to note that the MMP9–Carvacrol complex explores a much localized region in the conformational landscape. Moreover, the complex exhibits limited motions and predominantly adopts the same conformation. As for MMP9–Thymol, the conformational landscape shows high conformational diversity and flexibility; the system explores a wide area in PC2 as shown in **Figure 11**.

All the molecular dynamics analyses conducted in this study prove that Carvacrol stabilizes MMP9 better than Thymol. Lower RMSD and RMSF values, decreased radius of gyration, lesser SASA, hydrogen bonding, and conformational space restricted to a narrow region in the PCA plot suggest that Carvacrol leads to the formation of a more stable and compact MMP9 complex. Thus, the MD results confirm the molecular docking analysis.

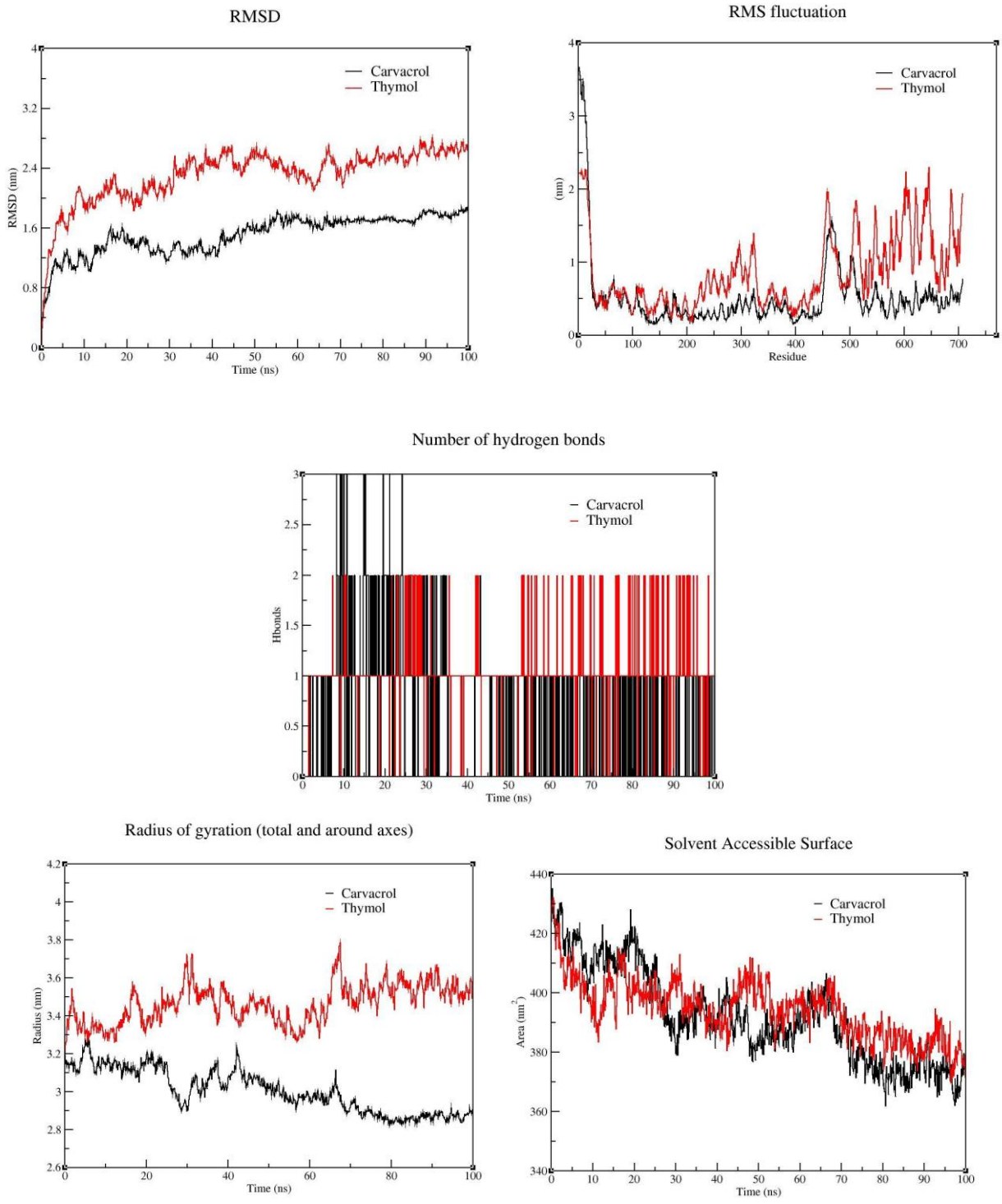

Figure 10. Molecular dynamics simulation analyses of MMP9 in complex with Carvacrol and Thymol over a 100 ns simulation period. (A) Root Mean Square Deviation (RMSD). (B) Root Mean Square Fluctuation (RMSF). (C) Radius of gyration (Rg). (D) Solvent-accessible surface area (SASA). (E) Hydrogen bond analysis. The black line represents the MMP9–Carvacrol complex, whereas the red line represents the MMP9-Thymol complex.

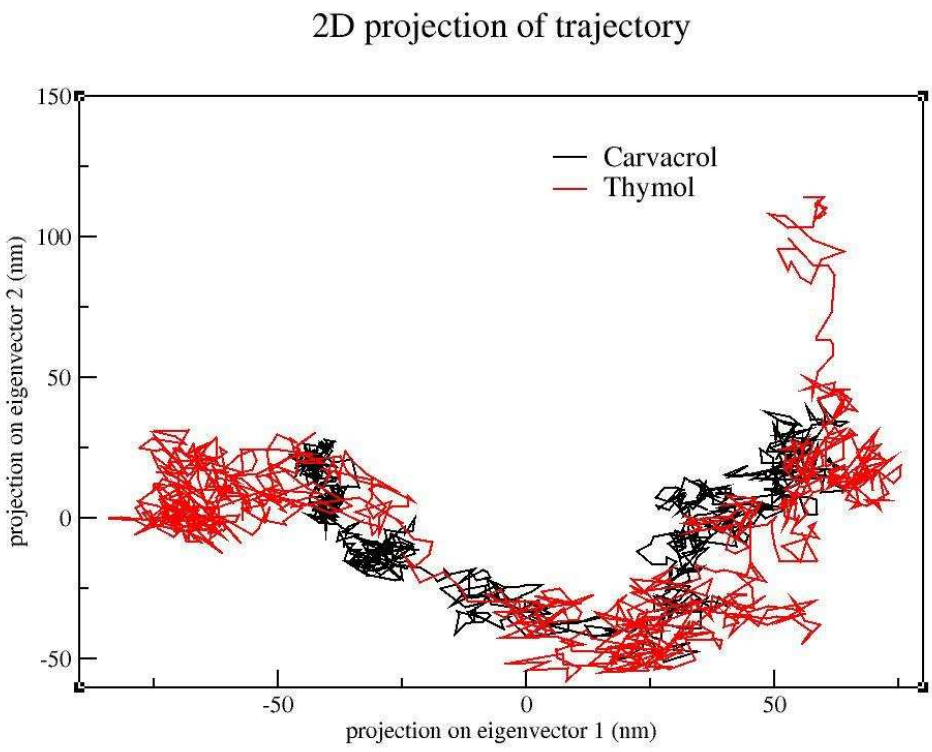

Figure 11. Principal component analysis (PCA) of the MMP9–Carvacrol and MMP9–Thymol complexes obtained from 100 ns molecular dynamics simulations. The black trajectory corresponds to the MMP9–Carvacrol complex, while the red trajectory corresponds to the MMP9–Thymol complex. The trajectories were projected onto the first two principal components (PC1 and PC2) to characterize the collective motions and conformational space sampled by the protein during the simulation. The distribution of conformational states reflects the dynamic behavior and structural flexibility of the respective protein–ligand complexes.

3.11 The Molecular Mechanics/Poisson-Boltzmann Surface Area

The MM-PBSA methodology was used to calculate the binding free energies of Carvacrol and Thymol, which can be broken down into individual energy components. Carvacrol showed a much better binding free energy (ΔG_{total} = −26.44 kcal/mol) than Thymol (ΔG_{total} = −14.68 kcal/mol), representing almost double the binding affinity, which is also coupled with the greater structural stability for the Carvacrol complex during the entire trajectory of the MD simulation (Figure 12).

Decomposition of the energy of the gas phase indicated that the binding was favoured by both van der Waals and electrostatic interactions in both systems. The van der Waals contribution to the two

ligands (Carvacrol: −32.91 kcal/mol; Thymol: −31.48 kcal/mol) was similar, indicating that these two isomeric phenols have a similar hydrophobic character in the MMP9 active site. The electrostatic contribution (ΔE_{EL}), however, was very favourable for Carvacrol (−12.12 kcal/mol) when compared to Thymol (−4.78 kcal/mol), which is about 7.3 kcal/mol. This difference implies that the hydroxyl and isopropyl groups in Carvacrol are able to interact more efficiently with the active site residues through polar interactions, which is a key factor in its higher total binding affinity. As a result, the aggregate gas phase energy of Carvacrol (ΔE_{gas} = −45.03 kcal/mol) was much higher than that of Thymol (ΔE_{gas} = −36.26 kcal/mol).

The components of the solvation free energy of the complexes showed that the major opposing (unfavourable) force in both complexes is the polar desolvation (ΔE_{GB}) term, typical of polar protein–ligand systems. The binding interface energy cost for desolvation, ΔE_{GB}, is lower for Carvacrol (+22.90 kcal/mol) than for Thymol (+26.01 kcal/mol), suggesting that the energetic cost of desolvation of Carvacrol binding interface is smaller. The nonpolar solvation terms (ΔESURF) were similar for both ligands (Carvacrol: −4.31 kcal/mol; Thymol: −4.43 kcal/mol), indicating a similar amount of nonpolar surface area being buried as a result of complex formation. The lower the solvation free energy that needs to be overcome to separate the two, the more thermodynamic favorable the reaction will be. The aggregate solvation free energies of Carvacrol and Thymol were +18.59 and +21.58, respectively, and the lower solvation free energy necessary to separate the two, the more thermodynamic favorable the reaction will be.

Electrostatic interactions and polar desolvation are identified as the major thermodynamic differences for Carvacrol and Thymol binding to MMP9 by the MM-PBSA analysis. Carvacrol was found to be the thermodynamically most favorable MMP9 inhibitor among the phytochemicals studied based on the three values obtained by summing together the three components, and this is also consistent with the molecular docking and molecular dynamics simulation results.

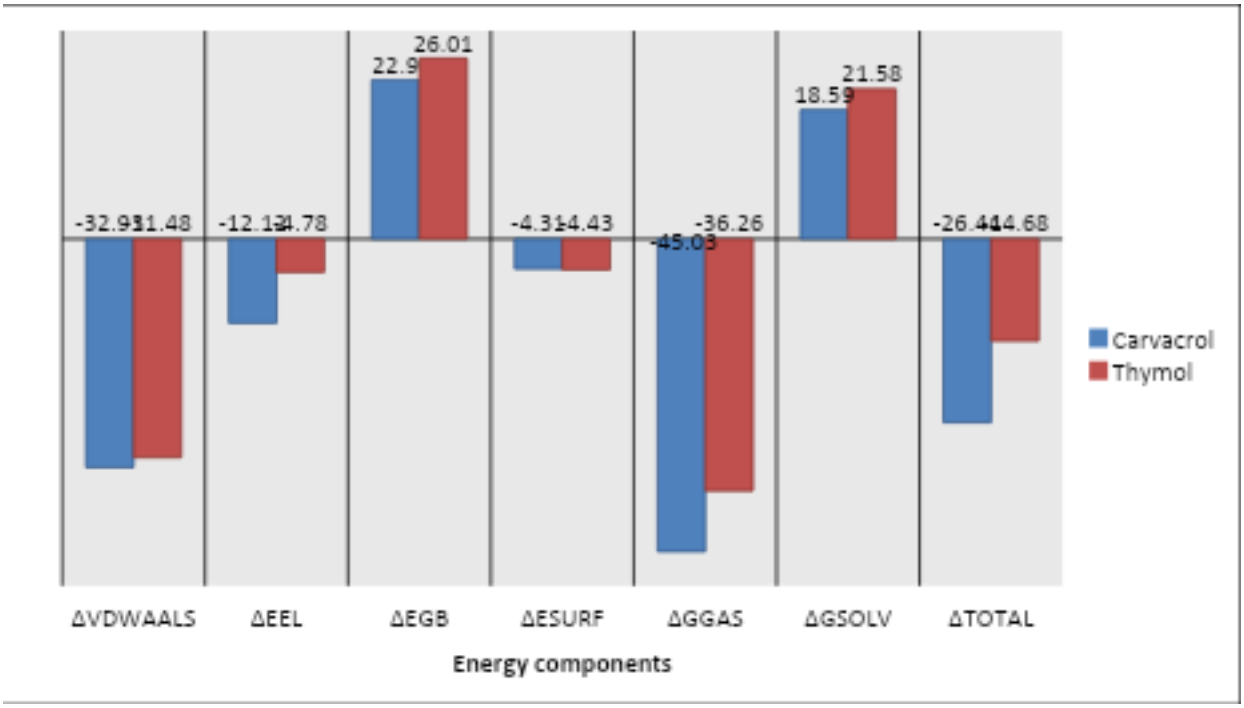

Figure 12: Comparative binding free energy of Thymol (Orange) and Carvacrol (Blue).

Table 6: Energy Component values of the phytochemicals: Carvacrol and Thymol

EnergyComponent	Carvacrol	Thymol
ΔVDWAALS	-32.91	-31.48
ΔEEL	-12.12	-4.78
ΔEGB	22.9	26.01
ΔESURF	-4.31	-4.43
ΔGGAS	-45.03	-36.26
ΔGSOLV	18.59	21.58
ΔTOTAL	-26.44	-14.68

3.12 Free Energy Landscape Analysis

To evaluate the thermodynamic stability and conformational dynamics of matrix metalloproteinase-9 (MMP9) upon binding with carvacrol and thymol, free energy landscape (FEL) analyses were performed based on the molecular dynamics simulation trajectories. The FEL

was projected onto the first two principal components (PC1 and PC2), with the Gibbs free energy (G) expressed in kJ/mol. In these representations, the deep blue regions indicate the lowest energy states, corresponding to the most stable global minima, while the red regions designate high-energy, transient conformational states. Analysis of the MMP9-carvacrol complex reveals a highly defined, V-shaped continuous energy valley. A prominent and concentrated global minimum (approximately 0 kJ/mol) is localized on one branch of the conformational space. The narrow, continuous nature of these energy basins suggests that the MMP9-carvacrol complex explores a highly restricted conformational space, ultimately settling into a stable, specific structural state with a maximum energy barrier of 9.74 kJ/mol. Conversely, the MMP9-thymol complex exhibits a noticeably broader and more distributed conformational landscape (**Figure 13**). Instead of a single dominant energy basin, the landscape is characterized by multiple distinct local minima spread across a wider, U-shaped pathway. This distribution indicates that the MMP9-thymol complex is relatively more flexible, fluctuating between several metastable sub-conformations rather than remaining locked in a single rigid state. The maximum energy barrier for this landscape is slightly lower at 9.17 kJ/mol, facilitating transitions between these multiple states. Overall, the FEL analyses demonstrate that carvacrol induces a more structurally rigid and stable complex with MMP9, whereas thymol permits greater structural flexibility and conformational sampling within the binding pocket.

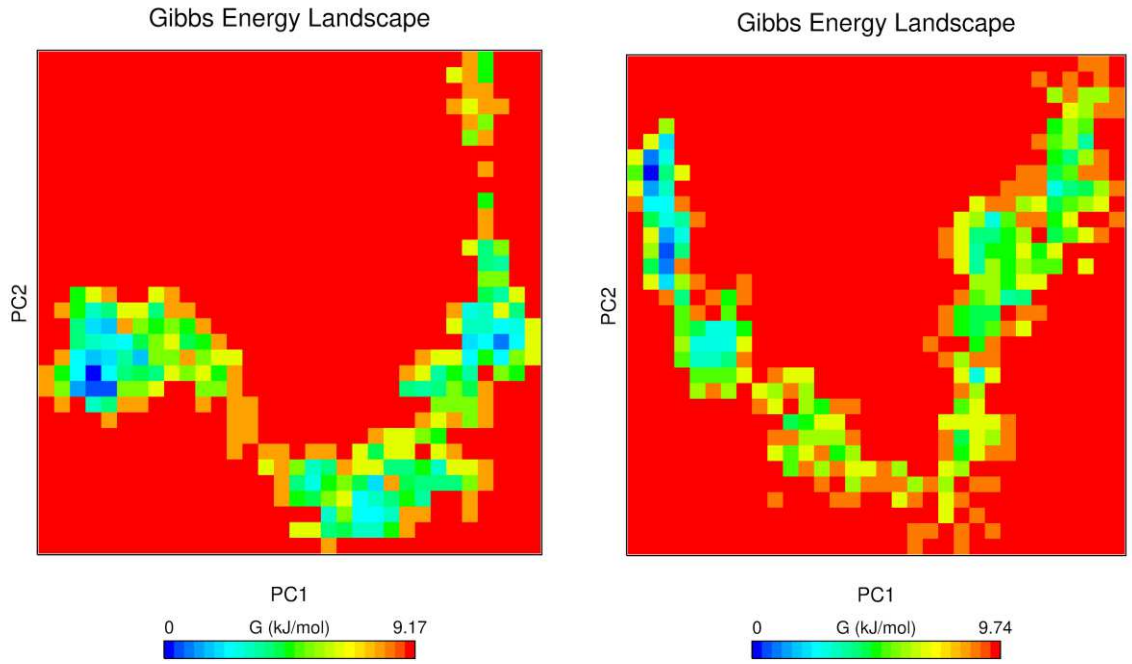

Figure 13: The Free Energy Landscape is projected onto the first two principal components (PC1 and PC2). The color scale represents the Gibbs free energy in kJ/mol, ranging from 0 (dark blue, stable states) to 9.17 (red, unstable states). The presence of multiple distinct deep energy basins indicates higher conformational flexibility and the existence of several metastable structural states compared to the carvacrol complex.

4. Discussion

Pancreatic ductal adenocarcinoma (PDAC) is a recalcitrant disease, driven by a convergent mutational architecture characterized by alterations of the genes KRAS, TP53, CDKN2A, and SMAD4, which will require agents able to target multiple oncogenic nodes to be effective as a monotherapy (Javadrashid et al., 2021; Mehra et al., 2021). To tackle this challenge, the study in the present work employed a computational approach that integrates network pharmacology, molecular docking, molecular dynamics (MD) simulation, free energy landscape (FEL) analysis and binding free energy quantification using MM-PBSA to systematically decipher the polypharmacological mechanisms of A. occidentale phytochemicals on PDAC. The integrated findings offer robust mechanisms and thermodynamics support of Carvacrol as a lead MMP9 inhibitor and offer a scientifically sound basis for the future development of these monoterpenoid scaffolds. From the 91 overlapping targets of A. occidentale phytochemicals and PDAC-associated genes, six hub proteins, AKT1, SRC, EGFR, STAT3, IL6 and MMP9, were identified in all three centrality metrics used (MCC, MNC and Betweenness centrality). The convergent multi-parameter identification is important because it suggests that these proteins are not only highly connected, but they also have topologically critical locations that act as gateways for the flow of information across the PDAC interactome. Mechanistically, the cross-referenced outputs as enrichment of the PI3K-Akt signaling pathway (hsa04151) are coherent with the key functional output of activation of AKT1, downstream of the activation of the KRAS gene via its constitutive activity (Liu, Wang, et al., 2020; Shi et al., 2023). Co-enrichment of the HIF-1 signaling pathway (hsa04066) and Focal adhesion pathway (hsa04510) further connects target activity of phytochemicals to hypoxic adaptation and ECM remodeling via integrin, respectively—two processes that cooperate to establish the PDAC invasive and metastatic phenotype. Particularly, A. occidentale bioactives may interact with the mechanisms underlying the failure of conventional targeted agents in PDAC, as this is revealed by the enrichment of pathways associated with drug resistance (hsa01521

Endocrine resistance and hsa01521 EGFR tyrosine kinase inhibitor resistance). Overall, the results are similar to previous network pharmacology analyses of multi-target natural products for PDAC, such as the analysis of emodin and triptolide, which were also found to target AKT1 and EGFR as network hubs (Liu, Zhao, et al., 2020; Shi et al., 2023).

Molecular docking studies were conducted against the six hub targets, and MMP9 was the most energetically favorable receptor for the A. occidentale monoterpenoid library, of the entire study, with Carvacrol having the highest binding affinity of the entire study (−7.767 kcal/mol). This value is in line with the docking scores obtained for other synthetic MMP9 inhibitors in similar computational campaigns, and Carvacrol is regarded as a scaffold, which is competitively strong (Santos et al., 2017). The interaction profiling showed that the superior binding of Carvacrol is due to a pivotal hydrogen bond with Met422 in the MMP9 active site, plus a rich hydrophobic interaction network with Leu397, His401, Leu418, Tyr423 and Arg424. Met422 is located near the catalytic zinc-binding motif of MMP9 and hydrogen bonding with this residue has been observed in successful MMP inhibitors, supporting the predicted binding mode. The structural isomer of Carvacrol, called thymol, which differs only in the position of hydroxyl group, also had a high affinity for MMP9 (−7.489 kcal/mol) and also had very similar hydrophobic contacts but its hydrogen bond was directed towards Tyr420, rather than Met422, which represents a slight change in binding geometry. This finding demonstrates the fact that slight conformational variations between the constitutional isomers can lead to significant variations in pharmacological activity and binding stability, which is consistent with the subsequent MD and MM-PBSA studies (Valdés-Tresanco et al., 2021). The 100 ns MD simulations were used for the aforementioned purpose, and showed that the docking predictions were dynamically validated for both complexes, allowing the discovery of largely different stability profiles for the two complexes of MMP9 (Abraham et al., 2015; Huang et al., 2017). The backbone RMSD analysis of MMP9–Carvacrol complex showed that the complex was at conformational equilibrium after 20 ns of simulation, and throughout the rest of the trajectory, the average of RMSD deviation was around 1.6 nm, with very little variation. The structural mobility of the MMP9–Thymol complex was in contrast significantly higher with RMSD values rising to c. 2.7 nm, and with continuous oscillations which did not allow a stable equilibrium plateau to be reached. This is an example of the differences in RMSD behavior, even though the initial docking obtained in both the isomers were very similar, explains why the dynamic simulation is important rather than the static docking for assessing true

binding competence. A complex that has a favourable docking energy but also a high structural lability, such as MMP9–Thymol, might be prone to frequent repositioning of the ligand, active site egress and/or displacement by physiological thermal energy, which would reduce the functional inhibitory effect in vivo. This interpretation was further supported by the per-residue RMSF analysis which showed that the MMP9–Carvacrol complex exhibited characteristic low Cα fluctuations throughout the protein, especially in the C-terminal domain (residues 450–700) that plays an important role in the protein function (Wu et al., 2024). The MMP9–Thymol complex complex, in contrast, showed several high amplitude RMSF peaks above 2.0 nm, suggesting that the binding of Thymol was not enough to limit the conformational freedom of the important protein domains. The RMSD and RMSF profiles demonstrate that Carvacrol results in a conformation of MMP9 that is more ordered and dynamically restricted, as would be expected in an active state with a productive and sustained interaction with the active site.

The results of the structural compactness parameters also gave supporting evidence for the better stabilizing capacity of Carvacrol. The solvent accessible surface area (SASA) of the MMP9–Carvacrol complex decreased progressively and monotonously from about 430 nm^2 to about 370 nm^2 during the simulation period, indicating ligand-induced conformational changes leading to a more compact and solvent protected protein structure. The progressive compaction is physically consistent with the burial of hydrophobic residues and closer packing at the protein–ligand interface. In contrast, the MMP9–Thymol complex showed relatively high and variable SASA values, suggesting that there is not a complete compaction, and it shows higher solvent exposure of internal residues (Vandooren et al., 2013). Thereafter, the radius of gyration (Rg) analysis showed that the Rg values of the Carvacrol complex slowly decreased from about 3.15 nm to 2.85 nm, whereas the Thymol complex had relatively stable Rg with higher values. The simultaneous decrease of both SASA and Rg values only in the Carvacrol complex suggests that the ligand causes real tertiary structural reorganization to a more compact and folded structure in the protein, rather than only filling the active site without having a global conformational effect. This compaction has been seen to be associated with increased thermodynamic stability and decreased susceptibility to MMP family member proteolytic degradation, providing added significance to the observation. The dynamics of the hydrogen bond was directly monitored for the persistence and quality of the protein–ligand contacts during the simulation. The complex MMP9 – Carvacrol forms three hydrogen bonds at the same time in the first 25 ns of the simulation and keeps 1-2

persistent contacts throughout the rest of the trajectory. The low RMSD profile suggests that Carvacrol is bound in a stable orientation relative to its position that does not change significantly, as indicated by the continuity of these hydrogen bonds. By contrast, the MMP9–Thymol complex mostly formed just one hydrogen bond and experienced many dissociation and association events along its trajectory. The hydrogen bonding network between Thymol and the receptor is just as intermittent and it is in this regard that the high structural lability of the ligand is correlated mechanistically with the high RMSD and RMSF values. Combined with the docking interaction data, these hydrogen bond dynamics help confirm that the interaction with Met422 is not a static, favorable dock interaction, but a dynamic persistent docking that is maintained under physiological temperature and pressure conditions. The conformational landscapes that each complex sampled were characterized in a global fashion using principal component analysis (PCA) of the MD trajectories. The MMP9–Carvacrol complex exhibited collective motion confined to a small, well-defined area of the PC1–PC2 phase space, suggesting a restricted range of motion and prevalent single stable conformation. The MMP9-Thymol complex, on the other hand, dispersed over a significantly larger conformational space, including significant excursions along PC2 to around 125 nm, indicative of high structural diversity and sampling of multiple conformational sub-states. The PCA projections were used to estimate the free energy landscape (FEL) of these differences, which gave a thermodynamic quantification of the differences. The MMP9–Carvacrol FEL showed a clear continuous energy valley with a single, well defined global energy minimum (≈0 kJ/mol) and a maximum energy barrier of 9.74 kJ/mol, typical of a very stable complex which is only able to sample a single dominant conformation. The topology of the MMP9–Thymol landscape, however, was wider, showing multiple local energy minima spread out in the basin with low barriers to inter-basin transitions (9.17 kJ/mol) and a metastable system that might sample multiple conformational sub-states. The lower energy barrier of the Thymol complex suggests that this complex should exhibit a lower kinetic stability compared to Carvacrol, such that the chances of thermal fluctuations taking the system out of its minimum energy conformation are increased at physiological temperature. Together, this PCA and FEL data illustrate that Carvacrol is not simply able to bind MMP9 more tightly, but it is actually able to change the accessible conformational space of the enzyme into one well-defined inhibited state. The thermodynamic resolution of differential stability profiles seen in MD simulations was obtained from quantitative binding free energy calculations performed with the MM-PBSA approach. The total binding free

energy of MMP9–Carvacrol complex was found to be ΔGtotal = −26.44 kcal/mol, whereas for MMP9–Thymol the ΔGtotal was found to be −14.68 kcal/mol, which is almost two-fold thermodynamic advantage for Carvacrol. It was found that this advantage is mainly due to a much more positive electrostatic contribution (ΔEEL: Carvacrol −12.12 kcal/mol vs Thymol −4.78 kcal/mol) which directly corresponds to the superior polar anchoring power of the hydroxyl group of Carvacrol at the contact point Met422 and hydrogen bond. The contributions of van der Waals forces were similar for the two isomers (-32.91 vs. -31.48 kcal/mol) as both possess almost identical molecular volume and hydrophobic surface area. Of particular interest is that the polar desolvation penalty (ΔEGB) for the binding of Carvacrol (+22.90 kcal/mol) was significantly lower than that of Thymol (+26.01 kcal/mol), due to the more favorable binding geometry of Carvacrol with the MMP9 binding site, which results in a lower thermodynamic cost for the desolvation of the binding interface. This is confirmed by the net solvation free energies (+18.59 and +21.58 kcal/mol for carvacrol and thymol, respectively). The energy decomposition analysis results per residue show that Met422, Leu397, Leu418, Tyr423, and Arg424 are the main contacts contributing to the binding of Carvacrol at the residue level, in line with the results of the static docking interaction profile, thus supporting that these contacts are thermodynamically productive and present during the simulation. The most stringent thermodynamic validation of Carvacrol as the leading MMP9 inhibitor in the phytochemical library of A. occidentale is provided by these MM-PBSA data.

The present study has its own set of limitations due to its purely computational approach. Although the ADME filtering pipeline was strict on the pharmacokinetic criteria, the predicted drug-likeness parameters are not substitutes for experimental absorption, bioavailability or metabolic stability (Daina et al., 2017). The desmoplastic microenvironment of PDAC, consisting of dense collagen networks and cancer-associated fibroblast activity, harbours many obstacles to drug penetration, which cannot be fully captured by in silico ADME models. Additionally, the MM-PBSA method gives accurate relative binding free energy for structurally similar ligands, but it neglects conformational entropy (−TΔS) and relies on a single-trajectory protocol which compromises the absolute energy accuracy. The SwissTargetPrediction prediction pipeline is probabilistic and might contain false positive associations or false negatives may occur, even though the targets are biologically relevant and have a low probability of association (Daina et al., 2017). The AKT1-directed activity of pulegone, while supported by favourable docking energetics and a plausible

interaction with the pleckstrin homology domain, was not further validated by MD simulation in this study; dynamic and thermodynamic confirmation of this interaction represents a priority for future computational work. Future research will thus need to focus on in vitro rigorous validation of the computational predictions, such as enzymatic inhibition assays using recombinant MMP9 and AKT1, cellular antiproliferative and invasion assays in PDAC cell lines (e.g., PANC-1, MIA PaCa-2), and eventually in vivo pharmacokinetic and efficacy study in orthotopic PDAC xenograft models to translate the computational predictions into empirically validated therapeutic candidates.

5. Conclusion

The present study provides a detailed multi-scale computational evaluation of anti-PDAC therapeutic potential of phytochemicals of Anacardium occidentale, which includes network-based target identification, molecular docking, molecular dynamics simulation and comprehensive thermodynamic binding free energy calculations. Network pharmacology performed systematic filtering of 399 phytochemicals through an ADME filter, resulting in a library of 146 drug-like phytochemicals, from which topologically critical hub targets were selected: AKT1, SRC, EGFR, STAT3, IL6 and MMP9, and which identified the main functional axes through which phytochemicals exert their activity against PDAC: PI3K-Akt, HIF-1, Focal adhesion. These results place the A. occidentale constituents as potential disruptors in the most clinically important oncogenic networks related to PDAC such as: survival signaling, hypoxic adaptation, ECM remodeling, and drug resistance mechanisms. Carvacrol was clearly identified as the most promising phytochemical compound with multiple targets from the evaluated phytochemical library. The high binding affinity to MMP9 (−7.767 kcal/mol) was confirmed dynamically and thermodynamically at all of the analytical levels used, with a persistent hydrogen bond with Met422 and a dense network of hydrophobic interactions supporting the binding interaction. MD simulation showed that it had lower RMSD (≤1.6 Å) of backbone atoms, a smaller per-residue RMSF, a more progressive compaction of structure (from SASA 430 to 370 nm^2; from Rg 3.15 to 2.85 nm), and more persistent hydrogen bonding (1-3 contact hydrogen bonding in continuous fashion) than its structural isomer Thymol. The binding of Carvacrol resulted in PCA and FEL results that clearly showed a very well-defined conformational state (single global minimum, energy barrier 9.74 kJ/mol), while the energy barrier for Thymol binding was 9.17 kJ/mol and the

results of PCA and FEL confirmed a multi-basin energy surface with multiple local minima. From the quantitative point of view, the MM-PBSA calculations demonstrated that Carvacrol has a thermodynamic advantage over Thymol, the differential energy being almost exclusively due to the better electrostatic interactions (ΔΔEEL ≈ 7.3 kcal/mol) and the lower polar desolvation penalty (ΔΔEpolar ≈ 3.77 kcal/mol). Complementarily, Pulegone exhibited the highest affinity to AKT1 (−6.960 kcal/mol) via numerous hydrophobic contacts with the pleckstrin homology domain, offering an alternate mechanistic pathway to inhibiting PI3K-Akt survival signaling. Five independent computational approaches – network pharmacology, molecular docking, molecular dynamics (MD) simulation, free energy landscape (FEL) analysis, and MM-PBSA – converged Carvacrol as the most promising phytochemical scaffold to be used as a MMP9-targeted molecule to intervene in the disease and Pulegone as a candidate for complementary AKT1-targeted intervention in PDAC. Multi-nodal intervention, targeting the three known activities they employ simultaneously – the invasion through MMP9, survival through AKT1, and adhesion signaling through SRC – is a mechanistically rational multi-nodal approach that meets the pharmacological requirements of PDAC. In conclusion, this investigation lays the foundation for an in silico evidence base of molecular mechanisms underpinning the claimed anti-PDAC properties of A. occidentale monoterpenoids and offers a solid basis for experimental testing. Next steps should involve in vitro enzymatic inhibition assays, antiproliferative and invasion studies using PDAC cell lines, and in vivo pharmacokinetics in orthotopic xenograft models, including studying capacity to reach therapeutic levels in the intratumoral environment, especially with regard to penetration of the desmoplastic stroma. The per-residue MM-PBSA hotspot map reported here is used for rational structural optimization of the Carvacrol and Pulegone scaffolds that focuses on increased electrostatic contacts with MMP9 (Met422) and hydrophobic contacts with AKT1 (Trp80/Leu210) – a chemistry forward strategy that enhances potency and selectivity. These results confirm that Anacardium occidentale is a biologically relevant route to explore as a source of structural motifs for future multi-targeted anti-PDAC drugs.

REFERENCES

1. Abraham, M. J., Murtola, T., Schulz, R., Páll, S., Smith, J. C., Hess, B., & Lindahl, E. (2015). GROMACS: High performance molecular simulations through multi-level

parallelism from laptops to supercomputers. Computer Physics Communications, 185(2), 199–206. https://doi.org/10.1016/j.cpc.2014.01.011

2. Ashburner, M., Ball, C. A., Blake, J. A., Botstein, D., Butler, H., Cherry, J. M., Davis, A. P., Dolinski, K., Dwight, S. S., Eppig, J. T., Harris, M. A., Hill, D. P., Issel-Tarver, L., Kasarskis, A., Lewis, S., Matese, J. C., Richardson, J. E., Ringwald, M., Rubin, G. M., & Sherlock, G. (2000). Gene ontology: Tool for the unification of biology. Nature Genetics, 25(1), 25–29. https://doi.org/10.1038/75556
3. Berman, H. M., Westbrook, J., Feng, Z., Gilliland, G., Bhat, T. N., Weissig, H., Shindyalov, I. N., & Bourne, P. E. (2000). The Protein Data Bank. Nucleic Acids Research, 28(1), 235–242. https://doi.org/10.1093/nar/28.1.235
4. Chen, Y., Zhang, H., Liu, X., & Wang, J. (2023). Network pharmacology and molecular docking analysis of Dendrobin A against pancreatic ductal adenocarcinoma. Frontiers in Pharmacology, 14, 1079539. https://doi.org/10.3389/fphar.2023.1079539
5. Chin, C.-H., Chen, S.-H., Wu, H.-H., Ho, C.-W., Ko, M.-T., & Lin, C.-Y. (2014). cytoHubba: Identifying hub objects and subnetworks from complex interactome. BMC Systems Biology, 8(Suppl. 4), S11. https://doi.org/10.1186/1752-0509-8-S4-S11
6. Daina, A., Michielin, O., & Zoete, V. (2017). SwissADME: A free web tool to evaluate pharmacokinetics, drug-likeness and medicinal chemistry friendliness of small molecules. Scientific Reports, 7, 42717. https://doi.org/10.1038/srep42717
7. Gfeller, D., Grosdidier, A., Wirth, M., Daina, A., Michielin, O., & Zoete, V. (2014). SwissTargetPrediction: A web server for target prediction of bioactive small molecules. Nucleic Acids Research, 42(W1), W32–W38. https://doi.org/10.1093/nar/gku293
8. Hess, B. (2008). P-LINCS: A parallel linear constraint solver for molecular simulation. Journal of Chemical Theory and Computation, 4(1), 116–122. https://doi.org/10.1021/ct700200b
9. Hosein, A. N., Brekken, R. A., & Maitra, A. (2020). Pancreatic cancer stroma: An update on therapeutic targeting strategies. Nature Reviews Gastroenterology & Hepatology, 17(8), 487–505. https://doi.org/10.1038/s41575-020-0300-1
10. Huang, J., Rauscher, S., Nawrocki, G., Ran, T., Feig, M., de Groot, B. L., Grubmüller, H., & MacKerell, A. D., Jr. (2017). CHARMM36m: An improved force field for folded and

intrinsically disordered proteins. Nature Methods, 14(1), 71–73. https://doi.org/10.1038/nmeth.4067

11. Javadrashid, D., Baghbanzadeh, A., Derakhshani, A., Leone, P., Silvestris, N., Racanelli, V., Solimando, A. G., & Baradaran, B. (2021). Pancreatic cancer signaling pathways, genetic alterations, and tumor microenvironment: The barriers affecting the method of treatment. Biomedicines, 9(4), 373. https://doi.org/10.3390/biomedicines9040373
12. Kanehisa, M., Furumichi, M., Sato, Y., Kawashima, M., & Ishiguro-Watanabe, M. (2023). KEGG for taxonomy-based analysis of pathways and genomes. Nucleic Acids Research, 51(D1), D587–D592. https://doi.org/10.1093/nar/gkac963
13. Kim, S., Chen, J., Cheng, T., Gindulyte, A., He, J., He, S., Li, Q., Shoemaker, B. A., Thiessen, P. A., Yu, B., Zaslavsky, L., Zhang, J., & Bolton, E. E. (2023). PubChem 2023 update. Nucleic Acids Research, 51(D1), D1373–D1380. https://doi.org/10.1093/nar/gkac956
14. Kuleshov, M. V., Jones, M. R., Rouillard, A. D., Fernandez, N. F., Duan, Q., Wang, Z., Koplev, S., Jenkins, S. L., Jagodnik, K. M., Lachmann, A., McDermott, M. G., Monteiro, C. D., Gundersen, G. W., & Ma'ayan, A. (2016). Enrichr: A comprehensive gene set enrichment analysis web server 2016 update. Nucleic Acids Research, 44(W1), W90–W97. https://doi.org/10.1093/nar/gkw377
15. Liu, J., Wang, Y., Ma, Y., & Yang, B. (2020). Identification of potential therapeutic targets in pancreatic adenocarcinoma using integrated bioinformatics analysis. BMC Medical Genomics, 13, 79. https://doi.org/10.1186/s12920-020-00737-5
16. Liu, X., Zhao, P., Wang, X., Wang, L., Zhu, Y., Song, Y., & Zhang, J. (2020). Triptolide inhibits pancreatic cancer by targeting PLAU based on network pharmacology analysis. European Journal of Pharmacology, 880, 173225. https://doi.org/10.1016/j.ejphar.2020.173225
17. Mehra, S., Deshpande, N., & Nagathihalli, N. (2021). Targeting PI3K pathway in pancreatic ductal adenocarcinoma: Rationale and progress. Cancers, 13(17), 4434. https://doi.org/10.3390/cancers13174434
18. Safran, M., Rosen, N., Twik, M., BarShir, R., Stein, T. I., Dahary, D., Fishilevich, S., & Lancet, D. (2021). The GeneCards suite. In Practical guide to life science databases (pp. 27–56). Springer.

19. Salentin, S., Schreiber, S., Haupt, V. J., Adasme, M. F., & Schroeder, M. (2015). PLIP: Fully automated protein–ligand interaction profiler. Nucleic Acids Research, 43(W1), W443–W447. https://doi.org/10.1093/nar/gkv315
20. Santos, R., Ursu, O., Gaulton, A., Bento, A. P., Donadi, R. S., Bologa, C. G., Karlsson, A., Al-Lazikani, B., Hersey, A., Oprea, T. I., & Overington, J. P. (2017). A comprehensive map of molecular drug targets. Nature Reviews Drug Discovery, 16(1), 19–34. https://doi.org/10.1038/nrd.2016.230
21. Shannon, P., Markiel, A., Ozier, O., Baliga, N. S., Wang, J. T., Ramage, D., Amin, N., Schwikowski, B., & Ideker, T. (2003). Cytoscape: A software environment for integrated models of biomolecular interaction networks. Genome Research, 13(11), 2498–2504. https://doi.org/10.1101/gr.1239303
22. Shi, Y., Zhang, X., Liu, W., & Li, H. (2023). Network pharmacology-based investigation of emodin against pancreatic adenocarcinoma. Frontiers in Oncology, 13, 1182453. https://doi.org/10.3389/fonc.2023.1182453
23. Sticht, C., De La Torre, C., Parveen, A., & Gretz, N. (2018). miRWalk: An online resource for prediction of microRNA binding sites. Nucleic Acids Research, 46(D1), D296–D302. https://doi.org/10.1093/nar/gkx1141
24. Szklarczyk, D., Kirsch, R., Koutrouli, M., Nastou, K., Mehryary, F., Hachilif, R., Gable, A. L., Fang, T., Doncheva, N. T., Pyysalo, S., Bork, P., Jensen, L. J., & von Mering, C. (2023). The STRING database in 2023: Protein–protein association networks and functional enrichment analyses for any sequenced genome of interest. Nucleic Acids Research, 51(D1), D638–D646. https://doi.org/10.1093/nar/gkad947
25. Trott, O., & Olson, A. J. (2010). AutoDock Vina: Improving the speed and accuracy of docking with a new scoring function, efficient optimization, and multithreading. Journal of Computational Chemistry, 31(2), 455–461. https://doi.org/10.1002/jcc.21334
26. Valdés-Tresanco, M. S., Valdés-Tresanco, M. E., Valiente, P. A., & Moreno, E. (2021). gmx_MMPBSA: A new tool to perform end-state free energy calculations with GROMACS. Journal of Chemical Theory and Computation, 17(10), 6281–6291. https://doi.org/10.1021/acs.jctc.1c00645
27. Vandooren, J., Van den Steen, P. E., & Opdenakker, G. (2013). Biochemistry and molecular biology of gelatinase B or matrix metalloproteinase-9 (MMP-9): The next

decade. Critical Reviews in Biochemistry and Molecular Biology, 48(3), 222–272. https://doi.org/10.3109/10409238.2013.770819

28. Vanommeslaeghe, K., Hatcher, E., Acharya, C., Kundu, S., Zhong, S., Shim, J., Darian, E., Guvench, O., Lopes, P., Vorobyov, I., & MacKerell, A. D., Jr. (2010). CHARMM General Force Field (CGenFF): A force field for drug-like molecules compatible with the CHARMM all-atom additive biological force fields. Journal of Computational Chemistry, 31(4), 671–690. https://doi.org/10.1002/jcc.21367
29. Wang, Z., Chen, Y., Wang, Y., & Zhang, H. (2020). Network pharmacology-based study on the mechanism of Qingyihuaji formula in pancreatic cancer treatment. Evidence-Based Complementary and Alternative Medicine, 2020, 3767094. https://doi.org/10.1155/2020/3767094
30. Wishart, D. S., Feunang, Y. D., Guo, A. C., Lo, E. J., Marcu, A., Grant, J. R., Sajed, T., Johnson, D., Li, C., Sayeeda, Z., Assempour, N., Iynkkaran, I., Liu, Y., Maciejewski, A., Gale, N., Wilson, A., Chin, L., Cummings, R., Le, D., & Wilson, M. (2018). DrugBank 5.0: A major update to the DrugBank database for 2018. Nucleic Acids Research, 46(D1), D1074–D1082. https://doi.org/10.1093/nar/gkx1037
31. Wu, N., Zhang, R., Peng, X., Fang, L., Chen, K., & Jestilä, J. S. (2024). Elucidation of protein–ligand interactions by multiple trajectory analysis methods. Physical Chemistry Chemical Physics, 26(11), 6903–6915. https://doi.org/10.1039/D3CP03492E
32. Zhang, Y., Li, X., Chen, H., & Zhao, W. (2022). Herbal medicine-derived compounds as potential therapeutic agents against pancreatic ductal adenocarcinoma. Scientific Reports, 12, 14174. https://doi.org/10.1038/s41598-022-14174-1
33. Zhang, Z., Wang, X., Liu, Y., & Huang, J. (2025). Cytotoxic phytochemicals and network pharmacology analysis in pancreatic cancer. Scientific Reports, 15, 18358. https://doi.org/10.1038/s41598-025-18358-3
34. Kalidass, B., & Muthukaliannan, G. K. (2026). In silico profiling of phytochemicals for modulating amyloid beta-mediated immune regulation and neuroinflammation in Alzheimer's disease. ACS Omega, 11(9), 14947–14963. https://doi.org/10.1021/acsomega.5c11503
35. Harakeh, S., Niyazi, H. A., Niyazi, H. A., Abdalal, S. A., Mokhtar, J. A., Almuhayawi, M. S., Alsharif, K. F., Alzahrani, K. J., Alharbi, S. A., Alghamdi, S. A., & Alhadrami, H. A.

(2024). Integrated network pharmacology approach to evaluate bioactive phytochemicals of Acalypha indica and their mechanistic actions to suppress target genes of tuberculosis. ACS Omega, 9(2), 2204–2219. https://doi.org/10.1021/acsomega.3c05589

36. Mathpal, S., Priyamvada, P., Ashok, G., Joshi, T., Saha, D., Mukherjee, A., Kumar, A., Singh, A., Sharma, P., & Gupta, R. (2025). Network pharmacology-driven investigation of luteolin from Annona muricata as a promising multi-target inhibitor for pancreatic cancer. Results in Chemistry, 16, 102506. https://doi.org/10.1016/j.rechem.2025.102506

AUTHOR INFORMATION

Corresponding Author

Janaki Ramaiah Mekala - *Department of Integrative Biology, School of Biosciences and Technology, Vellore Institute of Technology, School of Biosciences and Technology, Vellore Institute of Technology (VIT), Vellore - 632014, Tamil Nadu, India;* https://orcid.org/0000-0003-1814-2819; **Email:** janaki7777@gmail.com

Author

Anindita S Raju, Sadhana Balaji, Gayathri Chandran - *Department of Integrative Biology, School of Biosciences and Technology, Vellore Institute of Technology, School of Biosciences and Technology, Vellore Institute of Technology (VIT), Vellore - 632014, Tamil Nadu, India*

Author Contributions

Anindita S Raju - conceptualization, investigation, data collection, formal analysis, visualization, and writing of the original manuscript; Sadhana Balaji - manuscript review, editing, and scientific discussions; Gayathri Chandran - review, and editorial input; Janaki Ramaiah Mekala - project supervision, review and editing.

ACKNOWLEDGEMENTS

The authors would like to acknowledge Vellore Institute of Technology, Vellore for providing the facilities for carrying out this work. This work was financially supported from the Faculty Seed

Grant (RGEMS) Sanction order No: SG20250010, provided by Vellore Institute of Technology (VIT), Vellore.

DECLARATIONS

Conflict of Interests: The authors declare no conflict of interest.

Supplementary Files

This is a list of supplementary files associated with this preprint. Click to download.

- GRAPHICALABSTRACT.docx